Atmos. Chem. Phys., 14, 10465–10482, 2014
www.atmos-chem-phys.net/14/10465/2014/
doi:10.5194/acp-14-10465-2014

Atmospheric Chemistry and Physics
Open Access

Model-simulated trend of surface carbon monoxide for the 2001–2010 decade

J. Yoon and A. Pozzer

Atmospheric Chemistry Department, Max Planck Institute of Chemistry, P.O. Box 3060, 55020 Mainz, Germany

Correspondence to: J. Yoon (jongmin.yoon@mpic.de)

Received: 6 May 2014 – Published in Atmos. Chem. Phys. Discuss.: 14 May 2014
Revised: 11 August 2014 – Accepted: 27 August 2014 – Published: 1 October 2014

Abstract. We present decadal trend estimates of surface carbon monoxide (CO) simulated using the atmospheric chemistry general circulation model ECHAM5/MESSy (EMAC; ECHAM5 and MESSy stand for fifth-generation European Centre Hamburg general circulation model and Modular Earth Submodel System, respectively) based on the emission scenarios Representative Concentration Pathways (RCP) 8.5 for anthropogenic activity and Global Fire Emissions Database (GFED) v3.1 for biomass burning from 2001 through 2010. The spatial distribution of the modeled surface CO is evaluated with monthly data from the Measurements Of Pollution In The Troposphere (MOPITT) thermal infrared product. The global means of correlation coefficient and relative bias for the decade 2001–2010 are 0.95 and −4.29 %, respectively. We also find a reasonable correlation ($R = 0.78$) between the trends of EMAC surface CO and full 10-year monthly records from ground-based observation (World Data Centre for Greenhouse Gases, WDCGG). Over western Europe, eastern USA, and northern Australia, the significant decreases in EMAC surface CO are estimated at -35.5 ± 5.8, -59.6 ± 9.1, and -13.7 ± 9.5 ppbv decade^{-1}, respectively. In contrast, the surface CO increases by $+8.9 \pm 4.8$ ppbv decade^{-1} over southern Asia. A high correlation ($R = 0.92$) between the changes in EMAC-simulated surface CO and total emission flux shows that the significant regional trends are attributed to the changes in primary and direct emissions from both anthropogenic activity and biomass burning.

1 Introduction

Atmospheric carbon monoxide (CO) is a key tracer in atmospheric chemistry and climate change (Novelli et al., 1992; Forster et al., 2007; Duncan and Logan, 2008; Gomez-Pelaez et al., 2013). Major sources of atmospheric CO are fossil fuel combustion and biomass burning on the earth's surface (Wallace and Hobbs, 2006). CO leads to the formation of tropospheric ozone (O_3) and carbon dioxide (CO_2) through photochemical and oxidation reactions (Crutzen and Gidel, 1983; Fishman and Crutzen, 1978; Burrows et al., 1995). The main sink of CO is oxidation by hydroxyl radical (OH) and results in a moderately long lifetime (i.e., weeks to months) (Wallace and Hobbs, 2006). Because of this relatively short lifetime, CO is not well-mixed in the troposphere. It also controls the OH concentration and distribution (Levy, 1971; Thompson, 1992; Crutzen, 1974; Logan et al., 1981), which influences the oxidation of most trace gases on the earth (Khalil and Rasmussen, 1990), such as methane (CH_4) and other pollutants (Lelieveld et al., 2004; Novelli et al., 1992; Thompson and Cicerone, 1986). Therefore it contributes to climate change with direct and indirect radiative forcings around 0.024 and 0.2 W m^{-2}, respectively (Forster et al., 2007). Monitoring long-term series of surface CO is therefore important for understanding the influence of the direct CO emissions on atmospheric chemistry and, indirectly, on climate. Previous studies have shown that CO exhibited an increasing trend (worldwide) before the 1990s (Khalil and Rasmussen, 1988) and a decreasing trend (Novelli et al., 1994; Law, 1999), due to the primary decreases in anthropogenic emissions, thereafter (Duncan et al., 2007; Novelli et al., 2003). Duncan et al. (2007) and Duncan and Logan (2008) reported comprehensive results of the global/regional budget of CO and leading causes of its trends and interannual

variability from 1988 to 1997. Liu et al. (2010) looked into the internal variation of CO in the tropical troposphere using Aqua satellite data and the GEOS-Chem model in 2005 and 2006. There are no studies based on the model simulations that estimate recent changes (since 2000) in global CO.

The Measurements Of Pollution In The Troposphere (MOPITT) instrument is a nadir-viewing gas filter correlation spectrometer that has been measuring CO mixing ratios in the troposphere from the Terra satellite. It provides the long-term accumulated data of global CO that are the most suitable for the trend analysis because of their rigorous evaluation/validation (average errors for individual total column CO estimates: ±5–6 %) and 13-year continuous records since 2000 (University of Toronto and NCAR MOPITT Team, 1996; Pan et al., 1995, 1998; Worden et al., 2013). However, since the MOPITT-retrieved CO is based on climatology, its trend estimates can be significantly biased (Yoon et al., 2013). The ground-based observations can provide decades-long and highly accurate records using in situ measurement methods, but only for the available ground stations. Therefore, there is a significant limitation to estimate a reliable trend of global and regional surface CO from the study solely based on satellite-retrieved or ground-based data. In order to overcome this limitation, this study uses the ECHAM5/MESSy Atmospheric Chemistry (EMAC) model (Jöckel et al., 2010; ECHAM5 is the fifth-generation European Centre Hamburg general circulation model, and MESSy is the second version of the Modular Earth Submodel System), which can provide useful simulations to analyze chemical processes in the atmosphere and its interaction with the ocean and land surfaces.

In this study, the EMAC model is used to simulate surface CO trends from 2001 to 2010. The anthropogenic emissions are based on the Representative Concentration Pathways (RCP) 8.5 (Rihai et al., 2007) and the biomass burning emissions from the Global Fire Emissions Database (GFED) v3.1 (Giglio et al., 2010; van der Werf et al., 2010). The main objectives of this study are to analyze the long-term trend of global and regional surface CO, simulated using EMAC model, and to compare them to observationally derived trends. This paper is organized as follows: in Sect. 2, we describe the EMAC model and emission scenarios used for the global surface CO simulations from 2001 to 2010, and the MOPITT and WDCGG (World Data Centre for Greenhouse Gases) observations for the evaluations of spatial distribution and temporal change in the simulated surface CO. In Sect. 3, the model results are spatially and temporally evaluated through comparison with the observational data sets. In Sect. 4, we estimate the regional and global trends in EMAC-simulated surface CO and explore the major causes for the trends by comparing changes in CO direct emissions. Section 5 summarizes and presents our results and conclusions.

2 Model, emission scenarios, and observational data

2.1 ECHAM5/MESSy Atmospheric Chemistry (EMAC) model

The EMAC model is a numerical atmospheric chemistry general circulation model (ACGCM) developed for investigating atmospheric processes and their interaction with ocean, land, and human influences (see Jöckel et al. (2010) and publications at http://www.messy-interface.org/). It consists of ECHAM5 version 5.3.02 (Roeckner et al., 2006) and MESSy2 version 2.42 (Jöckel et al., 2010). The simulation results have been extensively evaluated with surface, aircraft, and satellite observations in many publications, such as Jöckel et al. (2006) and Pozzer et al. (2007, 2009, 2012a, b). In this study, a T63L31 resolution was used, corresponding to a horizontal resolution of approximately 1.875 by 1.875° in latitude and longitude and a vertical resolution of 31 levels from the surface to 10 hPa (i.e., vertical resolution: about 500 m in the lower troposphere, 750 m in the middle troposphere, and 1 km around the tropopause) (Roeckner et al., 2006).

2.2 Emission scenarios, RCP 8.5 and GFED v3.1

Several emission scenarios, e.g., the 1992 IPCC Scenarios (IS92) (Leggett et al., 1992) and Special Report on Emission Scenarios (SRES) (Nakicenovic et al., 2000), have been broadly used for the research on greenhouse gases, air pollutants, and future climate (e.g., Hogrefe et al., 2004; Jacobson and Streets, 2009). However, since they are the no-climate-policy scenarios, they fail to explore the impact of different climate policies (van Vuuren et al., 2011). The Fifth Intergovernmental Panel for Climate Change Assessment Report (IPCC AR5) gives an account of the concentration of greenhouse gases with respect to atmospheric radiation affected by anthropogenic activities (van Vuuren et al., 2011). The RCPs were developed by four individual modeling groups (i.e., NIES, IIASA, JGCRI, and PBL) (Riahi et al., 2007; van Vuuren et al., 2006, 2007, 2011). They consist of four emission scenarios also called RCP 2.6, 4.5, 6.0, and 8.5 representing the radiative forcing of anthropogenic activity from 2.6 to 8.5 $W m^{-2}$ in 2100, which depend on the mitigation or emission scenarios (van Vuuren et al., 2011). Among them, emission RCP 8.5 is used in this study to investigate the influence of anthropogenic activity on the change in surface CO from 2001 to 2010. It assumes that the emissions in greenhouse gases continue to increases post-2100 and their concentrations are stabilized post-2200 (Riahi et al., 2007; van Vuuren et al., 2011; Meinshausen et al., 2011). RCP 8.5 has been tested in Granier et al. (2011), which showed that it is a "reasonable" choice for anthropogenic emissions after the year 2000. Figure 1a shows the total mean of monthly emission flux of RCP 8.5 from 2001 and 2010. It illustrates that the high CO emissions due to anthropogenic activities

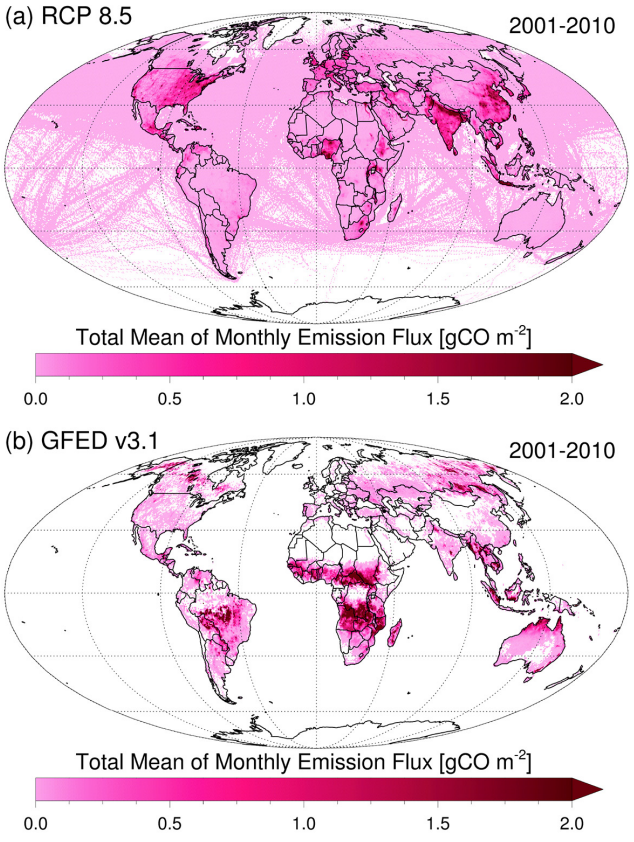

Figure 1. Global distributions of the total mean of monthly CO emission fluxes of **(a)** RCP 8.5 and **(b)** GFED v3.1 from 2001 to 2010.

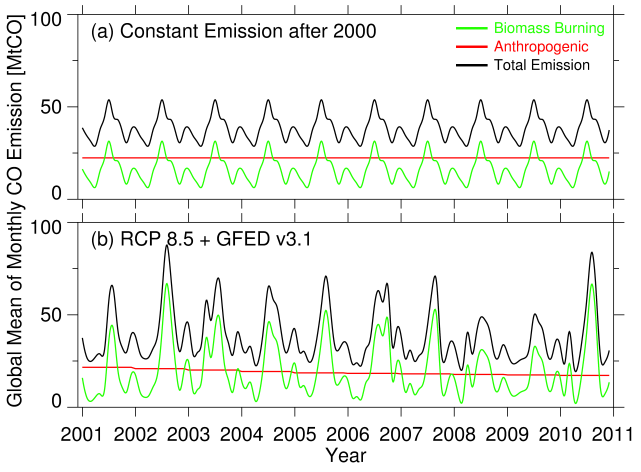

Figure 2. Time series of the global mean of monthly CO emissions: **(a)** constant emission of RCP 8.5 and GFED v3.1 after 2000 and **(b)** the combination of RCP 8.5 and GFED v3.1.

are located in highly populated regions or the largest urban megacities.

Fire is a significant emission source of several trace gases and aerosols, including atmospheric CO (Andreae and Merlet, 2001; Giglio et al., 2010). To consider the influence of CO emission from biomass burning, the GFED v3.1 is used in this study. It is based on global fire emissions from deforestation and savanna, forest, agricultural, and peat fires (van der Werf et al., 2010). Version 3 is updated using the combination of the long-term time series of improved satellite-derived data (e.g., burned area, fire activity, and plant productivity from the Moderate Resolution Imaging Spectroradiometer (MODIS), Tropical Rainfall Measuring Mission (TRMM), Visible and Infrared Scanner (VIRS), Along Track Scanning Radiometer (ATSR), and Advanced Very High Resolution Radiometer (AVHRR)) and model-estimated data (fuel loads and combustion completeness using the Carnegie–Ames–Stanford approach (CASA) biogeochemical model) from 1997 to 2009 (van der Werf et al., 2010). Figure 1b shows the global mean distribution of monthly GFED v3.1 surface CO emissions from 2001 to 2010 and shows that fire activity in/around tropical rainforests leads to large CO emissions. Direct CO emissions from anthropogenic activity and biomass burning represent around 50 % of the total CO budget (Granier et al., 1999; Duncan et al., 2007; Bergamaschi et al., 2000).

A simulation with constant emission (hereafter called CE scenario) is performed to assess only the possible influence of the meteorological transports on the surface CO trend as shown in Fig. 2a. Emissions in the model simulation CE are kept equal to the year 2000 from RCP 8.5 and GFED v3.1 for all 10 years of the simulation (2001–2010). In addition to the simulation CE, the combination of RCP 8.5 and GFED v3.1 (hereafter called RG scenario) in Fig. 2b is used for simulating a realistic surface CO concentration. It should be noted that, in RCP 8.5, CO emission does slightly decrease (globally) from the beginning of the 21st century (Butler et al., 2012). Chemistry and transport are fully decoupled, so both simulations have binary identical meteorology (i.e., transport). Additionally, the model has been weakly nudged towards analysis data of the European Centre for Medium-Range Weather Forecasts (ECMWF) (Jeuken et al., 1996) up to 100 hPa to obtain realistic model dynamics.

2.3 MOPITT Version 5 Level 3 thermal infrared CO

The Measurements of Pollution in the Troposphere (MOPITT) instrument, on board the EOS (Earth Observing System)-Terra spacecraft in 1999, has been providing continuous global products of CO total column values as well as vertical profiles of CO volume mixing ratio from 1000 to 100 hPa with a 100 hPa interval (Deeter et al., 2003). The global MOPITT-retrieved CO data with high accuracy (expected precisions: 10 %) have been applied to various studies on its sources, transports, and sinks (e.g., publications at http://www.acd.ucar.edu/mopitt/publications.shtml). In this study, the MOPITT Version 5 (V5) Level 3 (L3) thermal infrared (TIR) surface CO products in daytime are used

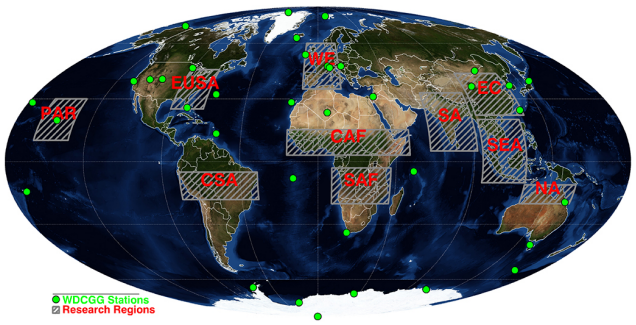

Figure 3. Research region domains and geolocations of WDCGG stations listed in Tables 1 and 2, respectively.

since they have been improved in the retrieval sensitivity and accuracy for the lower-tropospheric CO (Clerbaux et al., 2009; Worden et al., 2010, 2013; Deeter et al., 2013). MOPITT TIR products are based on thermal-infrared radiation at 4.7 µm. Even though a new joint (multispectral) TIR–NIR (near-infrared) product features the maximum sensitivity to near-surface CO, the TIR-based MOPITT can avoid significant random errors in NIR-based MOPITT products (near-infrared radiation at 2.3 µm). The grey hatched regions depicted in Fig. 3 and listed in Table 1, including the globe and the Northern and Southern Hemisphere, are selected for the spatial evaluation and trend estimates. These regions are important to monitor the surface CO released from anthropogenic and fire activities (see Fig. 1).

2.4 WDCGG surface CO

The WDCGG under the World Meteorological Organization – Global Atmosphere Watch (WMO–GAW; http://www.wmo.int/pages/prog/arep/gaw/gaw_home_en.html) was established in 1990 by the Japan Meteorological Agency (JMA) to assist in more reliable monitoring and analyzing of greenhouse (CO_2, CH_4, CFCs, N_2O, surface ozone, etc.) and related gases (CO, NO_x, SO_2, VOCs (volatile organic compounds), etc.) (http://ds.data.jma.go.jp/gmd/wdcgg/introduction.html). The WDCGG-archived CO data are categorized according to the observation platforms or analytical methods (see more details in GAW Report No. 188, WMO, 2009). The full 10-year monthly records of air sampling observations at the stationary platforms (shown as green dots in Fig. 3) were used to evaluate the temporal trend of EMAC-simulated surface CO. Detailed information about the station's geolocations, measurement methods, and contributors is listed in Table 2.

3 Evaluation of EMAC-simulated surface CO

3.1 Evaluation of spatial distribution using MOPITT V5 L3 TIR surface CO

It is quite challenging to retrieve tropospheric CO profiles based on mostly passive remote-sensing instruments (including MOPITT) because of a significant dependence on atmospheric temperature profile, surface pressure, and surface temperature in the retrieval algorithms (Deeter et al., 2003). In particular, without proper additional information, it is difficult to avoid the systematic error in the retrieved profiles from the algorithm that is developed based on climatology (i.e., a priori CO profiles) (Eskes and Boersma, 2003). This is why the averaging kernels, reflecting the relation between the retrieved and true profiles (Pan et al., 1998; Rodgers, 2000; Deeter et al., 2003), are important for a proper comparison between satellite-retrieved and model-simulated profiles (Rodgers, 2000; Rodger and Connor, 2003; Eskes and Boersma, 2003). The EMAC-simulated CO can be transformed into a quantity (so-called pseudo-retrieval, $\hat{\boldsymbol{x}}$) comparable to the MOPITT-retrieved CO as follows (Deeter et al., 2003, 2010):

$$\hat{\boldsymbol{x}} \cong \boldsymbol{x}_0 + \boldsymbol{A}\,(\boldsymbol{x} - \boldsymbol{x}_0) = \boldsymbol{A}\boldsymbol{x} + (\boldsymbol{I} - \boldsymbol{A})\,\boldsymbol{x}_0 \quad (1)$$

where $\boldsymbol{x}_0$, $\boldsymbol{A}$, $\boldsymbol{I}$, and $\boldsymbol{x}$ represent the MOPITT a priori CO, the MOPITT averaging kernels, the identity matrices, and the EMAC-simulated CO profiles from surface to 100 hPa, respectively. In this study, we transformed the EMAC-simulated surface CO into the surface pseudo-retrieval using the surface MOPITT a priori CO and averaging kernels matrix (Yoon et al., 2013).

The Taylor diagrams (Taylor, 2001; Forster et al., 2007; Meehl et al., 2007) in Fig. 4 show the spatial correlation coefficient (R), normalized standard deviation (SD), and normalized centered root-mean-square (RMS) difference for the different regions (see Fig. 3 and Table 1) and for the globe. This type of diagram can provide a concise statistical summary of spatial pattern correlation between satellite observation and model simulation (Taylor, 2001). The statistical quantities are listed in Table 3. In Fig. 4, the more closely the simulated pattern is located to the "Obs." on the x axis, the more closely it matches up with the observed spatial pattern. Additionally, the relative bias (B) is included in Fig. 4, allowing a more effective comparison between the spatial patterns of the monthly EMAC-simulated and MOPITT-observed CO. As shown again in Fig. 4b, the RG simulation results are more consistent with the MOPITT observations (i.e., in most regions, R is greater than about 0.9, less than about ± 0.25 of normalized SD, less than about 0.5 of normalized centered RMS difference, and less than about $\pm 10\,\%$ of B) than the one based on the CE scenario in Fig. 4a. Therefore, we can conclude that the simulation RG agrees well with the MOPITT-observed surface CO in the spatial distribution. Rather poor agreement in the Pacific Region (PAR) can be

Table 1. Geolocation and abbreviation of the regions considered in the evaluation of the spatial distribution and estimation of the regional and global trend of EMAC-simulated surface CO.

Region	Abbreviation	Latitude range	Longitude range
a. Pacific Region	PAR	10–30° N	165–145° W
b. Eastern USA	EUSA	25–45° N	90–70° W
c. Central South America	CSA	18–5° S	80–35° W
d. Western Europe	WE	35–60° N	10° W–15° E
e. Central Africa	CAF	3–15° N	18° W–53° E
f. Southern Africa	SAF	20–3° S	8E–42° E
g. Southern Asia	SA	5–33° N	65–92° E
h. Eastern China	EC	22–43° N	95–124° E
i. Southeastern Asia	SEA	10° S–20° N	95–120° E
j. Northern Australia	NA	20–11° S	120–150° E
k. Northern Hemisphere	NH	0–90° N	180° W–180° E
l. Southern Hemisphere	SH	90° S–0° N	180° W–180° E
m. Globe	GL	90° S–90° N	180° W–180° E

explained by the biases in the MOPITT CO surface retrievals at cleaner locations, such as over the Pacific Ocean (Emmons et al., 2004), and the failure to consider significant influences of natural sources (e.g., large-scale transport of tropospheric CO caused by the enhanced biomass burning due to El Niño; Chandra et al., 2009) in the EMAC model.

Figure 5 presents the global distributions of the seasonal MOPITT surface CO and pseudo-retrievals based on the EMAC-RG results from 2001 to 2010. The pseudo-retrieval is similar to the distribution of the remote-sensed MOPITT surface CO: the high concentration of surface CO emanating from the source regions over the eastern USA, western Europe, central Africa, and southern and eastern Asia is due to the combustion of fossil fuels and biomass burning (Wallace and Hobbs, 2006; Worden et al., 2013), while the CO transported by the atmospheric circulation can be detected over neighboring areas. To further analyze a spatial difference between the global distributions of seasonal MOPITT-retrieved and EMAC-simulated surface CO, we show the spatial difference in the third horizontal panel (Fig. 5c). In spring (MAM), the EMAC simulations over the eastern USA and western Europe dominantly influenced by anthropogenic emission are underestimated by 13.6 and 10.9 %, respectively, when compared to MOPITT. In contrast, the relative difference over southern Asia in autumn (SON) shows +16.5 %. The simulations over central Africa and southeastern Asia during the biomass burning seasons (i.e., summer (JJA) to autumn (SON)) are from +11.7 to +16.8 %. Generally the simulations are within ±10 % of the MOPITT observations, and therefore we can conclude that the EMAC-simulated surface CO based on the realistic RG scenario obviously shows good agreement with the MOPITT surface CO.

3.2 Evaluation of temporal change using WDCGG surface CO

In this section, the WDCGG surface CO observations at the stationary sites (see Fig. 3 and Table 2) are used to evaluate the temporal changes of EMAC simulations. We applied the monthly time series of EMAC-simulated and WDCGG-archived data (Y_t) to a linear trend model. The following form of a typical linear model has been adopted in various studies (Zhao et al., 2008; Hsu et al., 2012; de Meij et al., 2012; Yoon et al., 2014) for estimating climatological changes in the atmospheric system (Weatherhead et al., 1998, 2002):

$$Y_t = \mu + \omega X_t + S_t + N_t, \tag{2}$$

where μ, ω, and X_t denote the constant, the magnitude of the trend per year, and the years ($X_t = t/12$), respectively. S_t is a seasonal component fitted using Fourier analysis as follows:

$$S_t = \sum_{j=1}^{4} \left[\beta_{1,j} \sin\left(2\pi j t/12\right) + \beta_{2,j} \cos\left(2\pi j t/12\right)\right]. \tag{3}$$

N_t is the unexplained noise term, which is often assumed to be autocorrelated with one time lag (Weatherhead et al., 1998, 2002) as follows:

$$N_t = \phi N_{t-1} + \varepsilon_t, \tag{4}$$

where ϕ is the autocorrelation coefficient ($-1 < \phi < 1$) and ε_t is an independent random variable. If $\hat{\omega}$ denotes the trend estimate in Eq. (2), determined by minimizing the chi-square error statistic, the standard deviation ($\sigma_{\hat{\omega}}$) of the trend estimate can be quite accurately approximated as follows:

$$\sigma_{\hat{\omega}} \approx \frac{\sigma_\varepsilon}{(1-\phi)} \frac{1}{n^{3/2}} = \frac{\sigma_N}{n^{3/2}} \sqrt{\frac{1+\phi}{1-\phi}}, \tag{5}$$

Table 2. WDCGG stations providing full 10-year monthly records of surface CO from 2001 to 2010. The WDCGG-archived data are used for the evaluation of trend estimates in this study.

Station name	Latitude	Longitude	Country/ territory	Contributor	Instrument or analyses measurement method
Alert	82.5° N	62.5° W	Canada	CSIRO	GC-HgO
Ascension Island	7.9° S	14.4° W	UK	NOAA/ESRL	GC-HgO
Assekrem	23.3° N	5.6° E	Algeria	NOAA/ESRL	GC-HgO
Barrow	71.3° N	156.6° W	USA	NOAA/ESRL	GC-HgO
Cape Ferguson	19.3° S	147.1° E	Australia	CSIRO	GC- HgO
Cape Grim	40.7° S	144.7° E	Australia	CSIRO	GC-HgO
Cape Grim	40.7° S	144.7° E	Australia	NOAA/ESRL	GC-HgO
Cape Point	34.4° S	18.5° E	South Africa	SAWS	GC-other
Casey Station	66.3° S	110.5° E	Australia	CSIRO	GC- HgO
Halley Bay	75.6° S	26.5° W	UK	NOAA/ESRL	GC-HgO
Hegyhatsal	47.0° N	16.7° E	Hungary	NOAA/ESRL	GC-HgO
Heimaey	63.4° N	20.3° W	Iceland	NOAA/ESRL	GC-HgO
Izaña (Tenerife)	28.3° N	16.5° W	Spain	NOAA/ESRL	GC-HgO
Key Biscayne	25.7° N	80.2° W	USA	NOAA/ESRL	GC-HgO
Mace Head	53.3° N	9.9° W	Ireland	AGAGE	GC-MD
Mace Head	53.3° N	9.9° W	Ireland	NOAA/ESRL	GC-HgO
Macquarie Island	54.5° S	159.0° E	Australia	CSIRO	GC-HgO
Mahe Island	4.7° S	55.2° E	Seychelles	NOAA/ESRL	GC-HgO
Mauna Loa	19.5° N	155.6° W	USA	NOAA/ESRL	GC-HgO
Mt. Waliguan	36.23° N	100.9° E	China	NOAA/ESRL, CMA	GC-HgO
Niwot Ridge (T-van)	40.1° N	105.6° W	USA	NOAA/ESRL	GC-HgO
Park Falls	45.9° N	90.3° W	USA	NOAA/ESRL	GC-HgO
Palmer Station	64.9° S	64.0° W	USA	NOAA/ESRL	GC-HgO
Payerne	46.8° N	7.0° E	Switzerland	Empa	NDIR
Point Arena	39.0° N	123.7° W	USA	NOAA/ESRL	GC-HgO
Ragged Point	13.2° N	59.4° W	Barbados	NOAA/ESRL	GC-HgO
Rigi	46.1° N	8.5° E	Switzerland	Empa	NDIR
Ryori	39.0° N	141.8° E	Japan	JMA	GC-HgO
Sand Island	28.2° N	177.4° W	USA	NOAA/ESRL	GC-HgO
Sede Boker	31.1° N	34.9° E	Israel	NOAA/ESRL	GC-HgO
South Pole	90.0° S	24.8° W	USA	CSIRO	GC-HgO
South Pole	90.0° S	24.8° W	USA	NOAA/ESRL	GC-HgO
Syowa Station	69.0° S	39.6° E	Japan	NOAA/ESRL	GC-HgO
Tae-ahn Peninsula	36.7° N	126.1° E	Republic of Korea	NOAA/ESRL	GC-HgO
Tudor Hill	32.3° N	64.9° W	UK	NOAA/ESRL	GC-HgO
Tutuila (Cape Matatula)	14.2° S	170.6° W	USA	NOAA/ESRL	GC-HgO
Ulaan Uul	44.5° N	111.1° E	Mongolia	NOAA/ESRL	GC-HgO
Wendover	39.9° N	−113.7° W	USA	NOAA/ESRL	GC-HgO
Yonagunijima	24.5° N	123.0° E	Japan	JMA	GC-HgO
Zeppelinfjellet (Ny-Alesund)	79.0° N	11.9° E	Norway	NOAA/ESRL	GC-HgO

CSIRO: Commonwealth Scientific and Industrial Research Organisation (http://www.csiro.au/)
NOAA/ESRL: National Oceanic and Atmospheric Administration/Earth System Research Laboratory (http://www.esrl.noaa.gov/)
SAWS: South African Weather Service (http://www.weathersa.co.za/web/index.php)
AGAGE: Advanced Global Atmospheric Gases Experiment (http://agage.eas.gatech.edu/)
CMA: China Meteorological Administration (http://www.cma.gov.cn/en/)
JMA: Japan Meteorological Agency (http://www.jma.go.jp/jma/indexe.html)
Empa: Swiss Federal Laboratories for Materials Science and Technology (German acronym for Eidgenössische Materialprüfungs- und Forschungsanstalt) (http://www.empa.ch/)
GC-HgO: gas chromatography – mercuric oxide reduction detection
GC-MD: gas chromatography – multiple detectors
GC-other: gas chromatography (other)
NDIR: non-dispersive infrared gas analyzer

Table 3. Means ($\overline{CO}$) and corresponding statistic quantities* used in the comparison of spatial patterns (i.e., Taylor diagram in Fig. 4) in MOPITT-retrieved surface CO and pseudo-retrievals of EMAC-simulated surface CO.

Region	MOPITT-retrieved surface CO		Pseudo-retrieval of EMAC-simulated surface CO based on CE scenario					Pseudo-retrieval of EMAC-simulated surface CO based on RG scenario				
	$\overline{CO}$ [ppbv]	σ [ppbv]	$\overline{CO}$ [ppbv]	σ [ppbv]	R [unitless]	RMS [ppbv]	B [%]	$\overline{CO}$ [ppbv]	σ [ppbv]	R [unitless]	RMS [ppbv]	B [%]
PAR	91.78 ± 33.49	7.32 ± 5.28	78.05 ± 15.88	3.28 ± 2.82	0.45 ± 0.63	6.53 ± 5.86	-14.97 ± 15.72	86.66 ± 25.64	4.68 ± 4.47	0.69 ± 0.56	5.28 ± 3.23	-5.58 ± 10.06
EUSA	212.59 ± 83.20	68.62 ± 20.38	156.62 ± 24.81	56.16 ± 23.11	0.83 ± 0.23	37.81 ± 30.95	-26.33 ± 23.90	197.96 ± 48.06	66.63 ± 16.25	0.96 ± 0.04	19.97 ± 12.95	-6.88 ± 17.85
CSA	113.29 ± 78.23	38.85 ± 66.01	111.38 ± 56.94	35.71 ± 50.32	0.92 ± 0.12	15.59 ± 23.14	-1.68 ± 16.39	121.76 ± 82.84	45.99 ± 74.00	0.91 ± 0.13	19.14 ± 25.80	$+7.48 \pm 12.93$
WE	159.28 ± 47.53	30.35 ± 18.35	127.78 ± 25.46	27.74 ± 22.21	0.67 ± 0.42	23.56 ± 16.71	-19.78 ± 12.39	146.77 ± 36.01	28.22 ± 17.63	0.90 ± 0.12	13.15 ± 6.85	-7.85 ± 7.67
CAF	144.80 ± 89.62	48.61 ± 66.40	145.30 ± 88.66	63.57 ± 102.14	0.89 ± 0.15	30.55 ± 41.63	$+0.35 \pm 18.07$	154.74 ± 89.55	63.99 ± 96.87	0.93 ± 0.09	26.33 ± 32.73	$+6.86 \pm 18.10$
SAF	131.09 ± 83.03	45.83 ± 49.46	129.09 ± 61.08	44.95 ± 46.05	0.77 ± 0.36	30.86 ± 34.40	-1.53 ± 23.09	127.93 ± 67.17	47.06 ± 53.73	0.89 ± 0.12	21.34 ± 24.41	-2.41 ± 17.74
SA	148.30 ± 97.91	47.01 ± 30.33	125.09 ± 63.00	37.44 ± 25.01	0.87 ± 0.12	23.52 ± 20.34	-15.65 ± 19.05	164.62 ± 107.02	64.56 ± 46.64	0.94 ± 0.05	25.36 ± 21.47	$+11.00 \pm 16.06$
EC	251.16 ± 97.49	105.37 ± 51.19	176.03 ± 49.78	77.18 ± 39.77	0.74 ± 0.14	70.42 ± 39.08	-29.91 ± 14.74	244.31 ± 83.70	107.22 ± 57.33	0.91 ± 0.06	45.32 ± 21.73	-2.73 ± 14.23
SEA	132.01 ± 52.60	61.51 ± 50.05	133.78 ± 33.34	57.43 ± 44.83	0.89 ± 0.12	27.85 ± 29.05	$+1.34 \pm 19.27$	144.45 ± 47.70	72.66 ± 76.01	0.94 ± 0.06	25.68 ± 46.89	$+9.42 \pm 15.39$
NA	90.60 ± 38.02	17.15 ± 14.18	89.12 ± 15.11	13.32 ± 7.23	0.82 ± 0.19	9.84 ± 11.35	-1.64 ± 26.81	91.07 ± 31.94	16.06 ± 13.43	0.84 ± 0.22	9.43 ± 6.72	$+0.51 \pm 17.14$
NH	131.86 ± 40.93	48.95 ± 22.27	111.97 ± 24.17	39.46 ± 23.05	0.81 ± 0.13	28.90 ± 16.72	-15.08 ± 10.53	125.14 ± 33.00	48.63 ± 27.50	0.93 ± 0.03	18.43 ± 8.82	-5.10 ± 7.94
SH	67.89 ± 21.01	22.62 ± 19.06	73.08 ± 13.31	23.83 ± 13.33	0.86 ± 0.10	12.45 ± 6.67	$+7.64 \pm 13.67$	66.16 ± 19.04	25.44 ± 21.77	0.94 ± 0.06	9.03 ± 9.26	-2.54 ± 5.23
GL	99.80 ± 13.54	50.98 ± 22.70	92.30 ± 6.52	38.52 ± 16.30	0.87 ± 0.06	25.99 ± 13.24	-7.51 ± 7.05	95.52 ± 8.53	49.72 ± 20.84	0.95 ± 0.03	15.49 ± 5.17	-4.29 ± 5.58

* The statistic quantities are the mean values of monthly means ($\overline{CO}$), standard deviations (σ), spatial correlation coefficients (R), centered root-mean-square (RMS) differences, and relative biases (B) from 2001 to 2010 with a 95 % confidence interval ($\pm 2\sigma$).

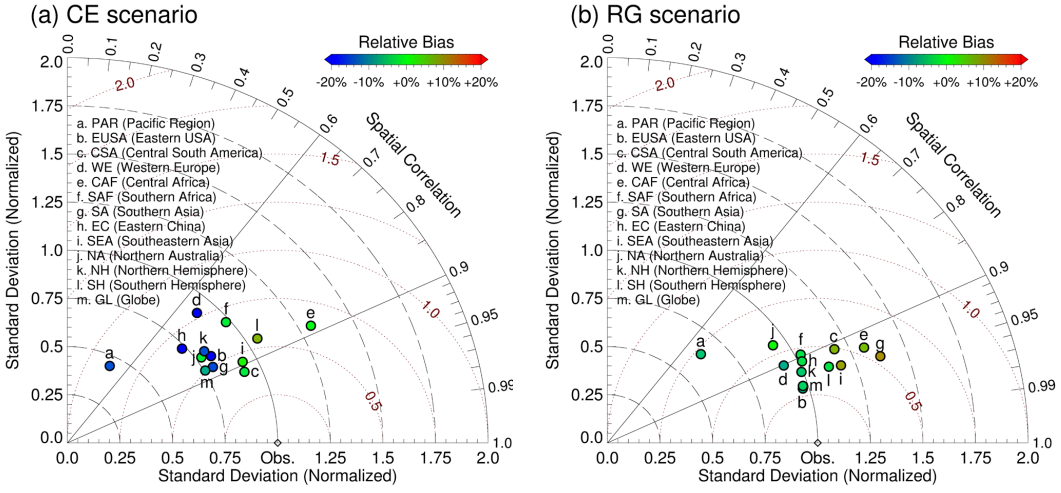

Figure 4. Spatial pattern analyses of the pseudo-retrievals of EMAC simulations based on **(a)** CE and **(b)** RG scenarios against MOPITT-retrieved surface CO for selected region domains listed in Table 1. The diagrams show the spatial correlation coefficients, normalized standard deviations, and normalized centered root-mean-square differences between the EMAC simulations and MOPITT observations. The standard deviation and centered root-mean-square difference are normalized to the variances of the observations. Detailed statistical quantities are summarized in Table 3.

where σ_ε, σ_N, and n denote the standard deviation of ε and N, and the number of years, respectively. In this study, we define $\hat{\omega}$ as a statistically significant trend at a 95 % confidence level when $\left|\hat{\omega}/\sigma_{\hat{\omega}}\right|$ is larger than 2 (Tiao et al., 1990; Weatherhead et al., 1998). This method is strictly applied to the full 10-year monthly records to minimize statistical biases from data inconsistencies in the trend estimates. In the same manner, the trends are derived from the EMAC-simulated surface CO data based on CE and RG scenarios at the grid closest to the WDCGG stations (see Table 2).

The trends of EMAC-simulated surface CO based on the RG scenario show better agreement and higher correlation (i.e., the correlation coefficient (R) and the slope of linear best-fit line (A) are 0.60 and 0.93 ± 0.40 in Fig. 6b) with the WDCGG trend than the ones based on the CE scenario ($R = -0.32$ and $A = -0.06 \pm 0.06$ in Fig. 6a). The specific values of trend estimates and statistical quantities are summarized in Table 4. At some stations (i.e., Cape Point, Key Biscayne, Niwot Ridge, Park Falls, Point Arena, Rigi, Sede Boker, and Tae-ahn Peninsula in Fig. 6b) influenced by local pollution or its transports, the trends of EMAC-simulated surface CO based on the RG scenario are considerably different to the WDCGG trends. It is attributed to the WDCGG flask sampling method, intended to minimize contamination from local pollution (Haas-Laursea and Hartley, 1997), and the rather low resolution of the EMAC model grid, which cannot discriminate between the local sources (Pozzer et al., 2007). Therefore, for such stations, we have not used the grid of EMAC-simulated surface CO closest to the WDCGG stations, but a model grid box oriented towards the upwind direction as suggested in Pozzer et al. (2007). Again, Fig. 7 presents the comparison between the trends of EMAC-simulated surface CO based on the RG scenario and WDCGG-archived surface CO. A better correlation coefficient and slope of linear best-fit line are obtained ($R = 0.78$ and $A = 0.94 \pm 0.25$). Therefore, we can conclude that the

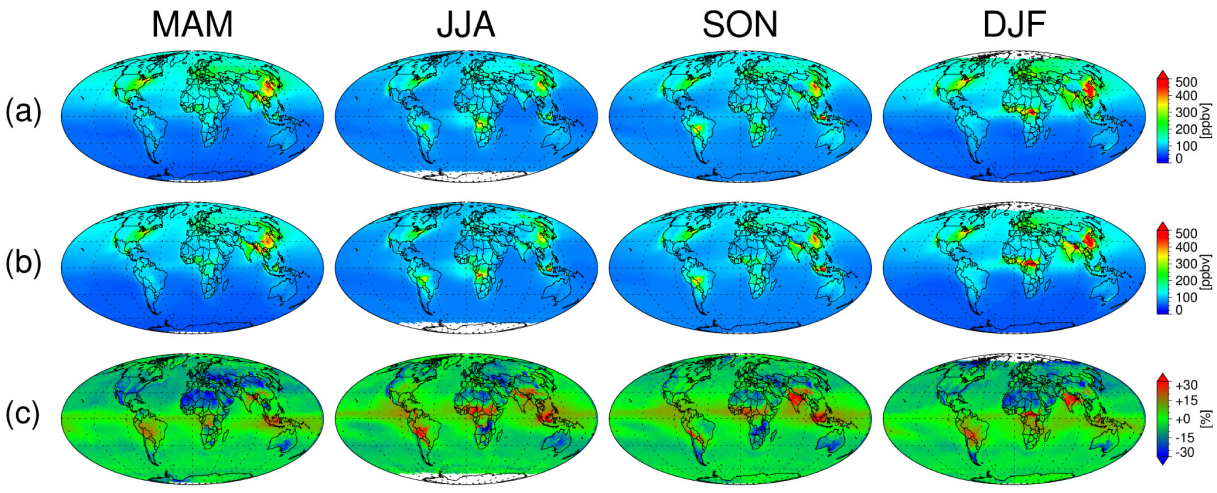

Figure 5. Global distributions of seasonal **(a)** MOPITT-retrieved surface CO, **(b)** pseudo-retrievals of EMAC-simulated surface CO based on RG scenarios, and **(c)** their relative difference between 2001 to 2010.

long-term simulations based on the RG scenario provide statistically reliable trend estimates of global surface CO.

4 Global and regional trend estimates of EMAC-simulated surface CO

4.1 Global scale

Novelli et al. (2003) reported that the global surface CO decreased by $-0.52\,\mathrm{ppb\,yr^{-1}}$ from 1991 to 2001. They explained the decline by the sharp decrease in CO (Dlugokencky et al., 1996) and the increase in surface atmospheric OH (Bekki et al., 1994) that followed the eruption of Mt. Pinatubo in June 1991. They also found that the decrease of CO ($-1.4\,\mathrm{ppbv\,yr^{-1}}$) in the northern extratropics was caused by the decrease in anthropogenic emissions in the Northern Hemisphere from 1991 to 2001, but there was no significant trend in the Southern Hemisphere. Similarly, Duncan and Logan (2008) found that the decrease in European emissions led to a decreasing trend ($-0.85\,\%\,\mathrm{yr^{-1}}$) in northern extratropics from 1988 to 1997. Worden et al. (2013) showed that the entire CO column still had a small negative trend in recent years (below $1\,\%\,\mathrm{yr^{-1}}$), from 2000 through 2011, with a strong decrease of CO over the US, Europe, and China, although it is not clear what is behind such trends.

Figure 8 presents the global trend of EMAC-simulated surface CO based on the CE and RG scenarios. The trends estimated in simulation CE could be attributed purely to dynamical changes as emissions and long-lived species are constant throughout the entire simulation. These trends (Fig. 8a) are statistically significant in the Southern Hemisphere and their magnitudes are relatively small. They are, however, not significant when changing emissions are included (simulation RG, Fig. 8b). In the realistic simulation RG (Fig. 8b), decreasing trends are generally predominant, in particular over Europe and the eastern USA as a result of strict environmental regulation (Streets et al., 2003; Yoon et al., 2011, 2014; Hilboll et al., 2013) and over southeastern Asia due to less fire activity (Giglio et al., 2010). They are consistent with the WDCGG-archived trends (see Sect. 3.2) as well as the decreasing trends in total CO columns retrieved from MOPITT and AIRS satellite instruments (MOPITT: $-1.44 \pm 0.44\,\%\,\mathrm{yr^{-1}}$ for Europe and $-1.42 \pm 0.40\,\%\,\mathrm{yr^{-1}}$ for the eastern USA; AIRS: $-1.00 \pm 0.66\,\%\,\mathrm{yr^{-1}}$ and $-0.96 \pm 0.36\,\%\,\mathrm{yr^{-1}}$, with $\pm 2\sigma$ errors, respectively) (Worden et al., 2013). In contrast, upward trends are estimated over quickly developing countries and forested regions (i.e., around southern Asia, eastern China, central South America, central and southern Africa). They can be attributed to the increase in anthropogenic and fire activities (Burrows et al., 1995; Bovensmann et al., 1999; Richter et al., 2005; Giglio et al., 2010). Novelli et al. (2003) and Duncan and Logan (2008) also reported a similar trend in northern extratropics influenced by the decrease in anthropogenic emissions in the Northern Hemisphere in the decade 1988–2001.

4.2 Regional scale

The sources of tropospheric CO are in situ oxidations and direct emissions: primarily oxidation of CH_4 ($\sim 800\,\mathrm{Tg\,CO\,yr^{-1}}$), emissions from biomass burning ($\sim 700\,\mathrm{Tg\,CO\,yr^{-1}}$) and fossil and domestic fuel ($\sim 650\,\mathrm{Tg\,CO\,yr^{-1}}$), and oxidation of NMHC (non-methane hydrocarbons) ($\sim 203\,\mathrm{Tg\,CO\,yr^{-1}}$) (Bergamaschi al., 2000; WMO, 1999; IPCC, 1996; Ehhalt et al., 2001; Duncan et al., 2007). In particular, the direct emissions alone account for around 50 % of the total CO budget (Ehhalt et al., 2001). In this section, we estimate the surface CO trends by region and compare them with the changes in direct emissions.

Table 4. Trend estimate ($\hat{\omega}$) and corresponding significance value ($|\hat{\omega}/\sigma_{\hat{\omega}}|$) of the WDCGG-archived and EMAC-simulated surface CO at a 95% confidence level. In this study, we define $\hat{\omega}$ as a statistically significant trend at a 95 % confidence level when $|\hat{\omega}/\sigma_{\hat{\omega}}|$ is larger than 2 (Tiao et al., 1990; Weatherhead et al., 1998).

Station	Contributor	WDCGG-archived surface CO		EMAC-simulated surface CO based on CE scenario		EMAC-simulated surface CO based on RG scenario	
		$\hat{\omega} \pm 2\sigma_{\hat{\omega}}$ [ppbv decade^{-1}]	$\lvert\hat{\omega}/\sigma_{\hat{\omega}}\rvert$ [unitless]	$\hat{\omega} \pm 2\sigma_{\hat{\omega}}$ [ppbv decade^{-1}]	$\lvert\hat{\omega}/\sigma_{\hat{\omega}}\rvert$ [unitless]	$\hat{\omega} \pm 2\sigma_{\hat{\omega}}$ [ppbv decade^{-1}]	$\lvert\hat{\omega}/\sigma_{\hat{\omega}}\rvert$ [unitless]
Alert	CSIRO	−26.29 ± 19.85	2.65	−1.40 ± 2.01	1.40	−15.75 ± 12.37	2.55
Ascension Island	NOAA/ESRL	+7.68 ± 5.99	2.56	−0.74 ± 2.19	0.68	+1.03 ± 4.29	0.48
Assekrem	NOAA/ESRL	−6.79 ± 6.89	1.97	−1.23 ± 3.30	0.75	−7.39 ± 4.64	3.19
Barrow	NOAA/ESRL	−15.01 ± 21.03	1.43	−1.32 ± 2.65	1.00	−14.22 ± 12.18	2.34
Cape Ferguson	CSIRO	−12.64 ± 10.26	2.47	−3.61 ± 3.58	2.01	−7.32 ± 5.71	2.56
Cape Grim	CSIRO	−6.02 ± 4.04	2.98	−1.40 ± 2.2	1.27	−2.79 ± 8.23	0.68
Cape Grim	NOAA/ESRL	+1.52 ± 5.06	0.60	−1.40 ± 2.2	1.27	−2.79 ± 8.23	0.68
Cape Point	SAWS	−10.23 ± 3.84	5.33	−3.35 ± 3.56	1.88	+6.62 ± 5.77	2.30
Casey Station	CSIRO	−6.26 ± 5.28	2.37	−2.25 ± 1.83	2.45	−0.98 ± 5.63	0.35
Halley Bay	NOAA/ESRL	−1.10 ± 4.61	0.47	−1.98 ± 1.76	2.26	−0.68 ± 5.34	0.25
Hegyhatsal	NOAA/ESRL	−52.26 ± 31.63	3.30	+2.12 ± 6.46	0.66	−52.73 ± 6.90	15.28
Heimaey	NOAA/ESRL	−13.54 ± 16.28	1.66	−1.51 ± 2.45	1.23	−17.68 ± 10.17	3.48
Izaña (Tenerife)	NOAA/ESRL	−4.89 ± 10.04	0.97	+0.02 ± 3.29	0.01	−13.02 ± 5.20	5.01
Key Biscayne	NOAA/ESRL	+5.03 ± 16.49	0.61	+3.40 ± 6.94	0.98	−15.14 ± 6.50	4.66
Mace Head	AGAGE	−9.059 ± 15.53	1.17	−2.51 ± 5.41	0.93	−22.39 ± 8.26	5.42
Mace Head	NOAA/ESRL	−18.81 ± 14.63	2.57	−2.51 ± 5.41	0.93	−22.39 ± 8.26	5.42
Macquarie Island	CSIRO	−5.35 ± 3.55	3.01	−2.38 ± 1.50	3.18	−1.15 ± 5.50	0.42
Mahe Island	NOAA/ESRL	+5.89 ± 10.85	1.08	−3.40 ± 3.43	1.98	−1.83 ± 4.96	0.74
Mauna Loa	NOAA/ESRL	−8.11 ± 11.40	1.42	−1.40 ± 2.45	1.14	−5.49 ± 4.89	2.25
Mt. Waliguan	NOAA/ESRL, CMA	−3.18 ± 24.61	0.26	−4.64 ± 11.22	0.83	−1.68 ± 12.61	0.27
Niwot Ridge (T−van)	NOAA/ESRL	−11.42 ± 11.89	1.92	−8.85 ± 8.33	2.12	−67.85 ± 9.97	13.61
Park Falls	NOAA/ESRL	−17.68 ± 15.16	2.33	−0.03 ± 8.77	0.01	−58.70 ± 11.67	10.06
Palmer Station	NOAA/ESRL	−0.05 ± 5.30	0.02	−2.21 ± 1.76	2.51	−0.94 ± 5.59	0.34
Payerne	Empa	−52.76 ± 22.21	4.75	+6.73 ± 9.53	1.41	−55.53 ± 7.60	14.61
Point Arena	NOAA/ESRL	−11.30 ± 14.28	1.58	−0.84 ± 13.39	0.13	−36.40 ± 19.73	3.69
Ragged Point	NOAA/ESRL	−0.84 ± 6.08	0.28	−0.35 ± 1.87	0.37	−3.24 ± 2.19	2.96
Rigi	Empa	−16.06 ± 19.39	1.66	−0.54 ± 11.34	0.10	−77.92 ± 9.02	17.27
Ryori	JMA	−8.26 ± 9.40	1.76	−3.54 ± 5.85	1.21	−17.47 ± 11.15	3.13
Sand Island	NOAA/ESRL	−8.65 ± 15.33	1.13	−2.21 ± 3.46	1.28	−7.31 ± 6.60	2.22
Sede Boker	NOAA/ESRL	−16.49 ± 15.68	2.10	+0.23 ± 6.14	0.08	+2.91 ± 7.11	0.82
South Pole	CSIRO	−6.65 ± 3.77	3.53	−2.04 ± 1.73	2.36	−0.74 ± 5.28	0.28
South Pole	NOAA/ESRL	+0.96 ± 5.38	0.36	−2.04 ± 1.73	2.36	−0.74 ± 5.28	0.28
Syowa Station	NOAA/ESRL	+0.08 ± 4.88	0.03	−2.21 ± 1.67	2.65	−0.91 ± 5.20	0.35
Tae-ahn Peninsula	NOAA/ESRL	+18.32 ± 36.25	1.01	+2.18 ± 16.26	0.27	−1.37 ± 20.77	0.13
Tudor Hill	NOAA/ESRL	−9.45 ± 12.53	1.51	+3.36 ± 4.34	1.55	−13.51 ± 5.81	4.65
Tutuila (Cape Matatula)	NOAA/ESRL	+2.39 ± 4.57	1.04	−3.15 ± 1.29	4.89	−2.93 ± 2.60	2.25
Ulaan Uul	NOAA/ESRL	−22.21 ± 32.76	1.36	−0.55 ± 6.57	0.17	−15.30 ± 22.40	1.37
Wendover	NOAA/ESRL	−11.05 ± 12.24	1.81	−5.43 ± 4.83	2.25	−27.26 ± 7.27	7.51
Yonagunijima	JMA	−8.50 ± 13.84	1.23	−4.97 ± 6.52	1.52	−6.73 ± 8.61	1.56
Zeppelinfjellet (Ny-Alesund)	NOAA/ESRL	−15.61 ± 19.50	1.60	−0.21 ± 2.33	0.18	−15.90 ± 10.49	3.03

Figure 9 shows the regional trends of EMAC-simulated surface CO for the selected regions (see Table 1 and Fig. 3), and Fig. 10 shows the corresponding changes in the emissions from anthropogenic activity and the biomass burning data set (i.e., RCP 8.5 and GFED v3.1).

The Pacific Region (PAR) is a remote area over open oceans and is the focus of many studies on climate change (e.g., Trenberth et al., 2002; Latif and Keenlyside, 2009; Rieder et al., 2013) since it is sensitive to El Niño and La Niña–Southern Oscillation (Rasmusson and Carpenter, 1982). Although PAR is almost not influenced by human activity, shipping transport in this region still plays a role in the CO concentration. The significant trend of EMAC surface CO is estimated to be -5.8 ± 5.5 ppbv decade^{-1} and is consistent with a significant trend of monthly anthropogenic emission (-0.007 ± 0.003 Mt CO decade^{-1}).

The eastern USA (EUSA) and western Europe (WE) are highly industrialized regions (Zhang et al., 2012; Yoon et al., 2011), where anthropogenic CO emissions are predominant (see Fig. 1a). Occasional influence from biomass burning is found, as shown in Fig. 10. As a result of environmental regulations over these regions in past decades (Streets et al., 2003; Yoon et al., 2011, 2012, 2014), the decreasing trends of atmospheric aerosol and short-lived trace gases have been reported in many studies (e.g., Smith et al., 2001; Streets et al., 2006; Richter et al., 2005; Hilboll et al., 2013). The dramatic decrease in EMAC surface CO is estimated to be -59.6 ± 9.1 ppbv decade^{-1} for EUSA and -35.5 ± 5.8 ppbv decade^{-1} for WE and is compatible (see Fig. 10) with the significant change in monthly emissions (-2.101 ± 0.328 Mt CO decade^{-1} for EUSA and -0.856 ± 0.036 Mt CO decade^{-1} for WE). These results are comparable to Worden et al. (2013) and Angelbratt et al. (2011), who derived the downward trends in MOPITT total-CO column ($(-3.14 \pm 0.88) \times 10^{16}$ molecules cm^{-2} yr^{-1} for eastern USA and $(-3.03 \pm 0.92) \times 10^{16}$ molecules cm^{-2} yr^{-1} for Europe) and solar FTIR (Fourier Transform InfraRed) partial-CO column (i.e., ∼ 0–15 km) (-0.45 ± 0.16 % yr^{-1}, -1.00 ± 0.24 % yr^{-1}, -0.62 ± 0.19 % yr^{-1}, and -0.61 ± 0.16 % yr^{-1} at the ground-based European stations Jungfraujoch, Zugspitze, Harestua, and Kiruna).

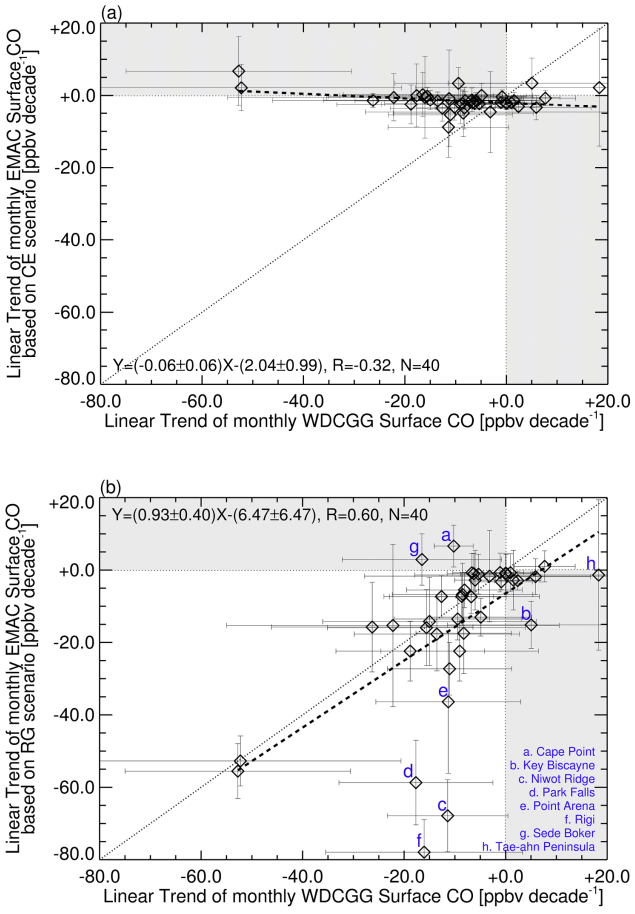

Figure 6. Comparisons of the trends of monthly EMAC-simulated surface CO based on **(a)** CE and **(b)** RG scenarios with the trend of monthly WDCGG-archived surface CO (with $\pm 2\sigma$ errors for selected WDCGG stations listed on Table 2). In particular in Fig. 6b, some stations (i.e., Cape Point, Key Biscayne, Niwot Ridge, Park Falls, Point Arena, Rigi, Sede Boker, and Tae-ahn Peninsula influenced by local pollution or transports) are selected as outliers and are indicated by blue fonts. Detailed values are summarized in Table 4.

Central South America, central and southern Africa, southeastern Asia, and northern Australia (i.e., CSA, CAF, SAF, SEA, and NA) are representative of the tropical rainforests (Ahlm et al., 2009; Held et al., 2005; Facchini et al., 2000; McFiggans et al., 2005). Over these regions, a large amount of surface CO has been emitted by biomass burning (see Figs. 1b and 12) through deforestation due to land use, subsistence agriculture, and spontaneous combustion in warm and dry seasons (Reeves et al., 2010; Johnson et al., 2008; Kirby et al., 2006; Davidson and Artaxo, 2004). Insignificant trends in EMAC-simulated surface CO are estimated over these regions ($+30.0 \pm 53.4$ ppbv decade^{-1} for CSA, $+2.2 \pm 7.4$ ppbv decade^{-1} for CAF, $+7.2 \pm 10.5$ ppbv decade^{-1} for SAF, and -21.3 ± 39.1 ppbv decade^{-1} for SEA) except in NA

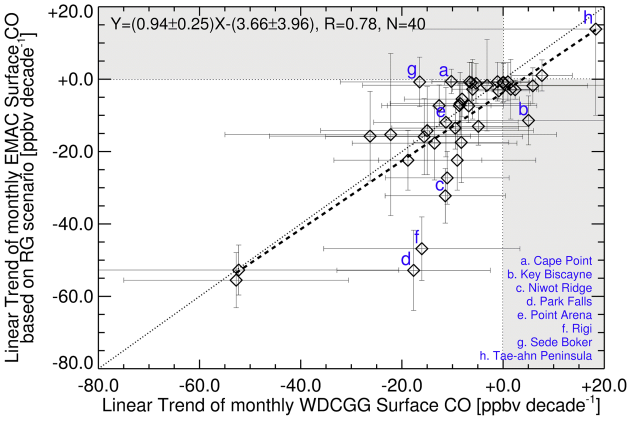

Figure 7. As in Fig. 6b but for the trends of monthly EMAC-simulated surface CO from a model grid box oriented towards the upwind direction at the stations.

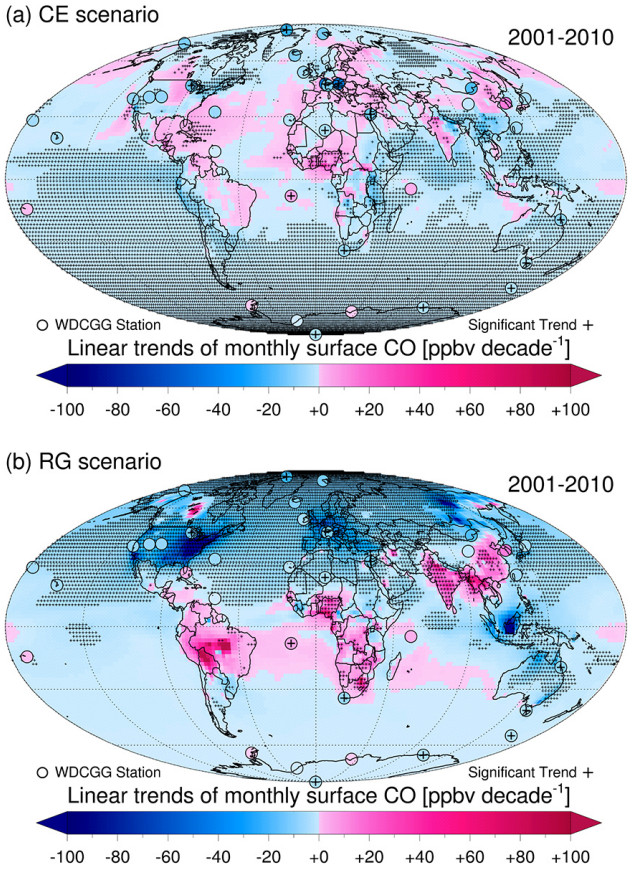

Figure 8. Global trend estimates of monthly WDCGG-archived and EMAC-simulated surface CO based on **(a)** CE and **(b)** RG scenarios from 2001 to 2010. The significant trends are shown as a plus symbol (+).

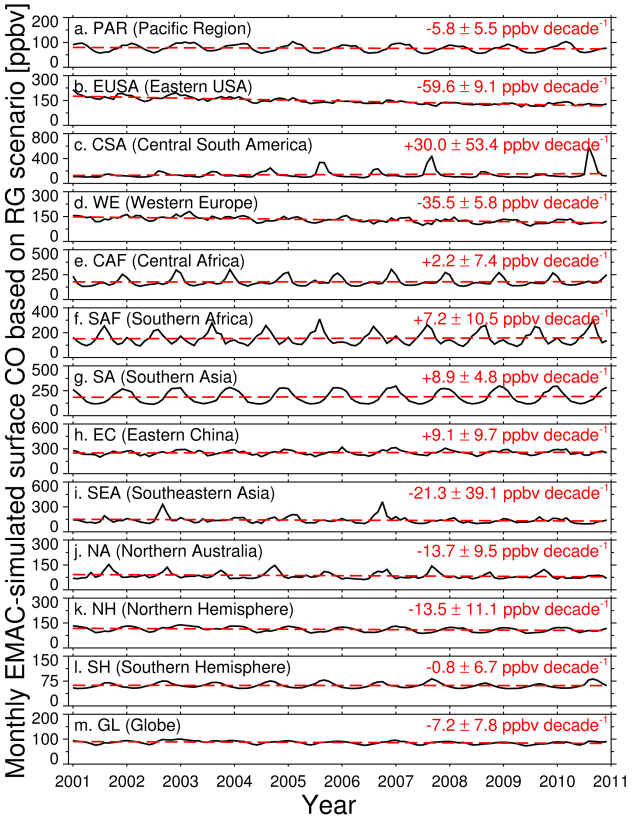

Figure 9. Regional and global trend estimates of monthly EMAC-simulated surface CO based on RG scenario with $\pm 2\sigma$ errors from 2001 to 2010.

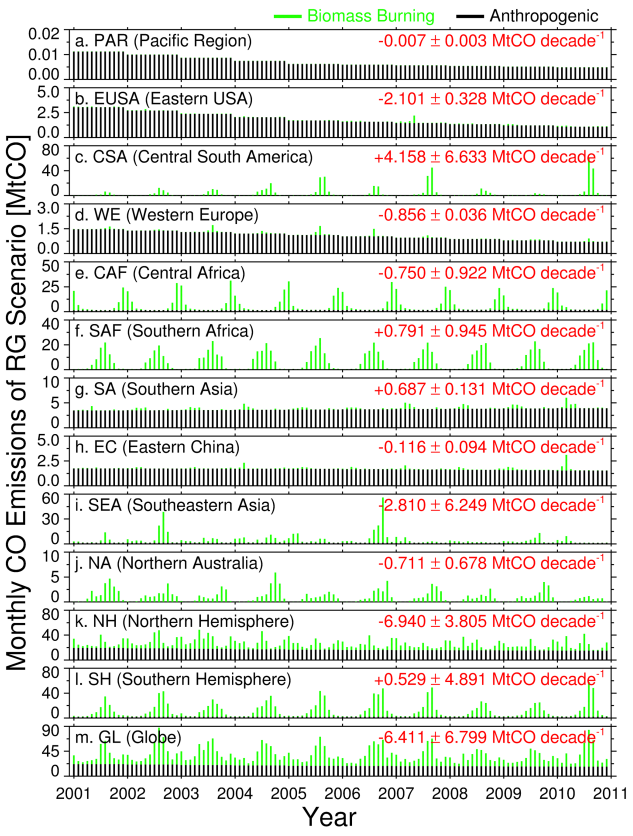

Figure 10. As in Fig. 9 but for ones of monthly RG CO emissions.

(-13.7 ± 9.5 ppbv decade^{-1}) because of the strong interannual variability of biomass burning emissions as shown in Fig. 10.

China and India are highly populated and developing countries home to about 36.5 % of the world population in 2013 (http://en.wikipedia.org/wiki/List_of_countries_by_population) and generating 14.1 % of world GDP in 2012 (World Bank Data, http://data.worldbank.org/). As a consequence, large amounts of anthropogenic pollutants (e.g., aerosols, nitrogen dioxide, sulfur dioxide, and surface ozone) that lead to environmental and health problems are emitted into the atmosphere (Ohara et al., 2007; Pozzer et al., 2012a, b; Lelieveld et al., 2013). The long-term change in these pollutants has been a key issue in many studies (e.g., Yoon et al., 2014; Richter et al., 2005; Lu et al., 2010; Xu et al., 2008). The increase in EMAC surface CO is estimated in both regions to be $+8.9 \pm 4.8$ ppbv decade^{-1} for SA and $+9.1 \pm 9.7$ ppbv decade^{-1} for eastern China (EC). In the case of EC, since the trend is not statistically significant and is the opposite of the decreasing trend in the emission (-0.116 ± 0.094 Mt CO decade^{-1}), it is influenced by the changes in transport or secondary chemical production (Tohjima et al., 2014; Angelbratt et al., 2011).

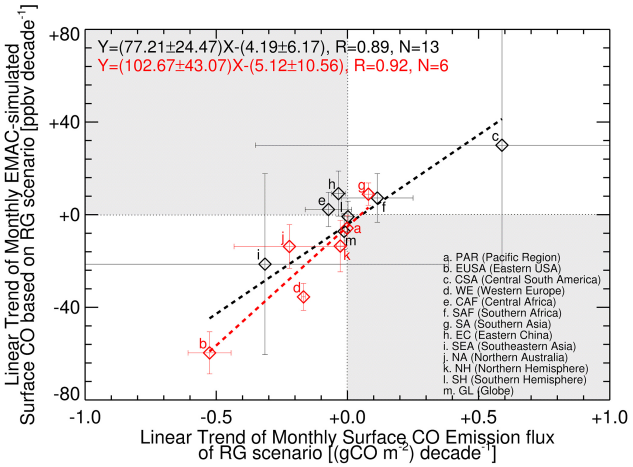

Figure 11. Comparisons of the trends of monthly RG CO emission flux against the trend of monthly EMAC-simulated surface CO with $\pm 2\sigma$ errors for the selected regions listed oin Table 1. Black and red fonts indicate the results of the comparison between all available trends and of the comparison between significant trends only, respectively.

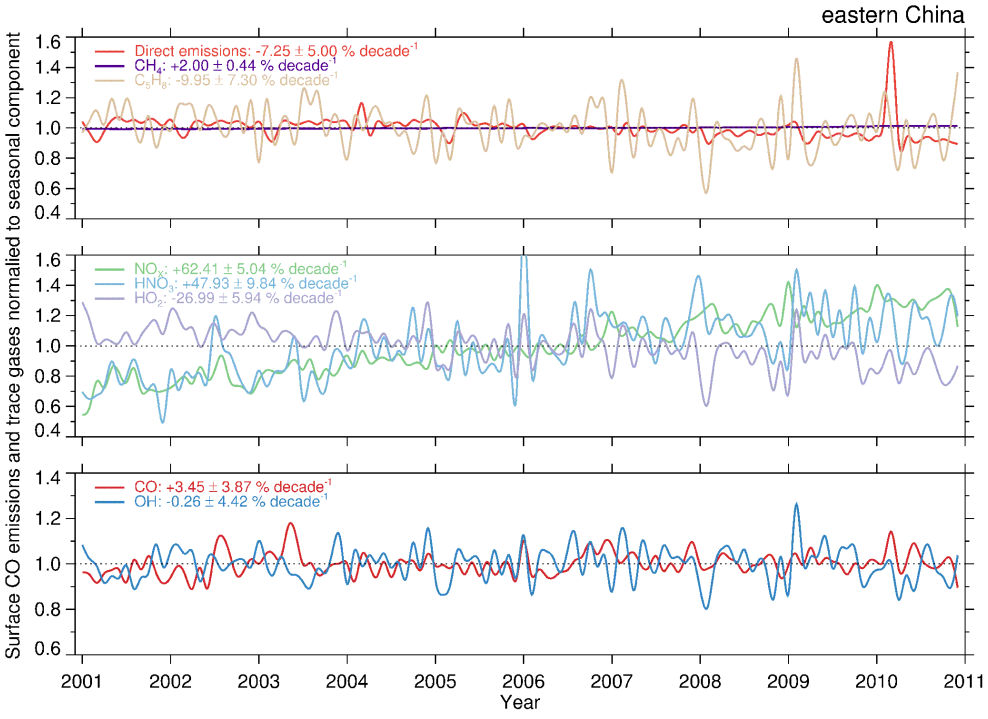

Figure 12. Long-term time series of surface CO emissions and relevant trace gases normalized to seasonal component over eastern China from 2001 to 2010.

On a global scale, the simulation RG shows a significant trend only in the NH (-13.5 ± 11.1 ppbv decade^{-1} for the NH, -0.8 ± 6.7 ppbv decade^{-1} for the SH, and -7.2 ± 7.8 ppbv decade^{-1} for the globe (GL)). Notably, the evident change in NH CO is attributed to the significant change in emissions (-6.940 ± 3.805 MtCO decade^{-1}). Figure 11 clearly shows a high correlation between the trends in EMAC-simulated surface CO and total emission flux ($R = 0.88$ between all trends and $R = 0.92$ between significant trends). Since the trends of WDCGG-archived surface CO are highly correlated with the EMAC-simulated trends as shown in Fig. 8, we can confirm that the changes in surface CO over the past decade are mostly due to changes in the emissions.

Notwithstanding a significant decrease in the CO emissions over eastern China, the simulated trend in surface CO shows an insignificant increase. This is the opposite of the results from Worden et al. (2013) that showed a negative trend in MOPITT tropospheric column CO over eastern China. This inconsistency can be explained, as CO is not only controlled by emissions but also by its chemistry (oxidation and chemical formation). For example, OH is the main oxidant of many trace gases and therefore one of the most important species in atmospheric chemistry (Lawrence et al., 2001; Wallace and Hobbs, 2006). CO removal from the troposphere occurs almost exclusively by reaction with OH (Hauglustaine et al., 1998; IPCC, 1996), and, on the other hand, CO provides the most important sink for OH (Lelieveld et al., 2002; Thompson, 1992). Figure 12 shows long-term time series of surface CO emissions and trace gases from the simulation RG relevant to the chemical production of CO and OH over eastern China from 2001 to 2010. As mentioned, the direct emissions from biomass burning and fossil and domestic fuel generally have the most influence on surface CO change and show a significantly negative trend in the eastern China region (-7.25 ± 5.00 % decade^{-1}). Oxidation of CH_4 is the primary chemical source for CO, and the surface CH_4 increases significantly ($+2.00 \pm 0.44$ % decade^{-1}). In contrast, isoprene (C_5H_8), an oxidation products that is another important source of CO (Holloway et al., 2000), changes by -9.95 ± 7.30 % decade^{-1}. These trends show that both direct emissions and chemical formation of CO over the EC region generally decreased during the decade 2001–2010.

However, surface NO_x drastically increased during the same decade ($+62.41 \pm 5.04$ % decade^{-1}), which contributed to the decrease in the HO_x level (-26.99 ± 5.94 % decade^{-1} for HO_2 and -0.26 ± 4.42 % decade^{-1} for OH) via the formation of HNO_3 ($+47.93 \pm 9.84$ % decade^{-1}) (see also Lelieveld et al., 2002, 2004). The decrease in OH concentration yields a reduced oxidation of CO and, therefore, the presence over the EC region of a slightly positive trend of CO. It must be underlined that this trend is not significant, and it is calculated only for the surface. The total tropospheric column of CO is strongly influenced by the long-range transport of CO, which has a lifetime of around 1 month.

The results of simulation CE, where the pure CO transport induces a slight negative trend in the CO concentration over EC, are therefore in agreement with the results of Worden et al. (2013).

5 Summary and conclusion

The global and regional changes in surface CO have been estimated using the EMAC model for 2001 to 2010. The spatial distributions and temporal changes in the EMAC-simulated surface CO based on CE and RG scenarios have been extensively evaluated with results derived from MOPITT-retrieved and WDCGG-archived data. We have shown that the spatial distribution and temporal change of EMAC-simulated surface CO based on the RG scenario are consistent with the observational data sets. Significant trends in EMAC surface CO have been found in the Northern Hemisphere (confirming the decreasing trends already reported in the northern extratropics in the decade 1988–2001), in particular, a decreasing trend over the eastern USA, western Europe, and an increasing trend over southern Asia, mostly due to the changes in anthropogenic emission. In contrast, over the regions influenced by biomass burning (i.e., central South America, central Africa, southern Africa, and southeastern Asia), no significant trend has been detected because of a high interannual variability of fire activity.

Acknowledgements. The authors would like to thank the NASA Langley Research Center (Atmospheric Science Data Center, https://eosweb.larc.nasa.gov/) and World Data Centre for Greenhouse Gases (WDCGG, http://ds.data.jma.go.jp/gmd/wdcgg/) for providing the MOPITT Version 5 TIR Level 3 products and monthly WDCGG-archived surface CO data used in the study. We gratefully acknowledge the efforts of the EMAC development team to develop and make available the EMAC modeling system.

The service charges for this open access publication have been covered by the Max Planck Society.

Edited by: B. N. Duncan

References

Ahlm, L., Nilsson, E. D., Krejci, R., Mårtensson, E. M., Vogt, M., and Artaxo, P.: Aerosol number fluxes over the Amazon rain forest during the wet season, Atmos. Chem. Phys., 9, 9381–9400, doi:10.5194/acp-9-9381-2009, 2009.

Andreae, M. O. and Merlet, P.: Emission of trace gases and aerosols from biomass burning, Global Biogeochem. Cy., 15, 955–966, doi:10.1029/2000GB001382, 2001.

Angelbratt, J., Mellqvist, J., Simpson, D., Jonson, J. E., Blumenstock, T., Borsdorff, T., Duchatelet, P., Forster, F., Hase, F., Mahieu, E., De Mazière, M., Notholt, J., Petersen, A. K., Raffalski, U., Servais, C., Sussmann, R., Warneke, T., and Vigouroux, C.: Carbon monoxide (CO) and ethane (C_2H_6) trends from ground-based solar FTIR measurements at six European stations, comparison and sensitivity analysis with the EMEP model, Atmos. Chem. Phys., 11, 9253–9269, doi:10.5194/acp-11-9253-2011, 2011.

Bekki, S., Law, K. S., and Pyle, J. A.: Effect of ozone depletion on atmospheric methane and CO concentrations, Nature, 371, 595–597, doi:10.1038/371595a0, 1994.

Bergamaschi, P., Hein, R., Heimann, M., and Crutzen, P. J.: Inverse modeling of the global CO cycle: 1. Inversion of CO mixing ratios, J. Geophys. Res.-Atmos., 105, 1909–1927, doi:10.1029/1999JD900818, 2000.

Bovensmann, H., Burrows, J. P., Buchwitz, M., Frerick, J., Noël, S., Rozanov, V. V., Chance, K. V., and Goede, A. P. H.: SCIAMACHY – Mission Objectives and Measurement Modes. J. Atmos. Sci., 56, 127–150, doi:10.1175/1520-0469(1999)056<0127:SMOAMM>2.0.CO;2, 1999.

Buchwitz, M., de Beek, R., Bramstedt, K., Noël, S., Bovensmann, H., and Burrows, J. P.: Global carbon monoxide as retrieved from SCIAMACHY by WFM-DOAS, Atmos. Chem. Phys., 4, 1945–1960, doi:10.5194/acp-4-1945-2004, 2004.

Buchwitz, M., de Beek, R., Noël, S., Burrows, J. P., Bovensmann, H., Bremer, H., Bergamaschi, P., Körner, S., and Heimann, M.: Carbon monoxide, methane and carbon dioxide columns retrieved from SCIAMACHY by WFM-DOAS: year 2003 initial data set, Atmos. Chem. Phys., 5, 3313–3329, doi:10.5194/acp-5-3313-2005, 2005.

Buchwitz, M., Khlystova, I., Bovensmann, H., and Burrows, J. P.: Three years of global carbon monoxide from SCIAMACHY: comparison with MOPITT and first results related to the detection of enhanced CO over cities, Atmos. Chem. Phys., 7, 2399–2411, doi:10.5194/acp-7-2399-2007, 2007.

Burrows, J. P., Hölzle, E., Goede, A. P. H., Visser, H., and Fricke, W.: SCIAMACHY – Scanning Imaging Absorption Spectrometer for Atmospheric Chartography, Acta Astronaut., 35, 445–451, 1995.

Burrows, J. P., Goede, A. P. H., Muller, C., and Bovensmann, H.: SCIAMACHY – The Need for Atmospheric Research from Space, in: SCIAMACHY – Exploring the Changing Earth's Atmosphere, edited by: Gottwald, M. and Bovensmann, H., Springer Science + Business Media B.V., Dordrecht, the Netherlands, 1–17, doi:10.1007/978-90-481-9896-2_1, 2011.

Butler, T. M., Stock, Z. S., Russo, M. R., Denier van der Gon, H. A. C., and Lawrence, M. G.: Megacity ozone air quality under four alternative future scenarios, Atmos. Chem. Phys., 12, 4413–4428, doi:10.5194/acp-12-4413-2012, 2012.

Chandra, S., Ziemke, J. R., Duncan, B. N., Diehl, T. L., Livesey, N. J., and Froidevaux, L.: Effects of the 2006 El Niño on tropospheric ozone and carbon monoxide: implications for dynamics and biomass burning, Atmos. Chem. Phys., 9, 4239–4249, doi:10.5194/acp-9-4239-2009, 2009.

Clerbaux, C., Hadji-Lazaro, J., Payan, S., Camy-Peyret, C., and Mégie, G.: Retrieval of CO columns from IMG/ADEOS spectra, IEEE T. Geosci. Remote, 37, 1657–1661, 1999.

Clerbaux, C., Boynard, A., Clarisse, L., George, M., Hadji-Lazaro, J., Herbin, H., Hurtmans, D., Pommier, M., Razavi, A., Turquety, S., Wespes, C., and Coheur, P.-F.: Monitoring of atmospheric composition using the thermal infrared IASI/MetOp sounder, Atmos. Chem. Phys., 9, 6041–6054, doi:10.5194/acp-9-6041-2009, 2009.

Crutzen, P. J.: Photochemical reactions initiated by and influencing ozone in unpolluted tropospheric air, Tellus, 26, 47–57, 1974.

Crutzen, P. J. and Gidel, L. T.: A two-dimensional photochemical model of the atmosphere. 2: The tropospheric budgets of anthropogenic chlorocarbons CO, CH_4, CH_3Cl and the effect of various. NO_x sources on tropospheric ozone, J. Geophys. Res., 88, 6641–6661, 1983.

Davidson, E. A. and Artaxo, P.: Globally significant changes in biological processes of the Amazon Basin: Results of the Large-scale Biosphere-Atmosphere Experiment, Global Change Biol., 10, 1–11, doi:10.1111/j.1529-8817.2003.00779.x, 2004.

Deeter, M. N., Emmons, L. K., Francis, G. L., Edwards, D. P., Gille, J. C., Warner, J. X., Khattatov, B., Ziskin, D., Lamarque, J.-F., Ho, S.-P., Yudin, V., Attié, J.-L., Packman, D., Chen, J., Mao, D., and Drummond, J. R.: Operational carbon monoxide retrieval algorithm and selected results for the MOPITT instrument, J. Geophys. Res., 108, 4399, doi:10.1029/2002JD003186, 2003.

Deeter, M. N., Edwards, D. P., Gille, J. C., and Drummond, J. R.: Sensitivity of MOPITT observations to carbon monoxide in the lower troposphere. J. Geophys. Res., 112, 24306, doi:10.1029/2007JD008929, 2007.

Deeter, M. N., Edwards, D. P., Gille, J. C., Emmons, L. K., Francis, G., Ho, S.-P., Mao, D., Masters, D., Worden, H., Drummond, J. R., and Novelli, P. C.: The MOPITT version 4 CO product: Algorithm enhancements, validation, and long-term stability, J. Geophys. Res., 115, D07306, doi:10.1029/2009JD013005, 2010.

Deeter, M. N., Worden, H. M., Gille, J. C., Edwards, D. P., Mao, D., and Drummond, J. R.: MOPITT multispectral CO retrievals: Origins and effects of geophysical radiance errors, J. Geophys. Res., 116, D15303, doi:10.1029/2011JD015703, 2011.

Deeter, M. N., Worden, H. M., Edwards, D. P., Gille, J. C., and Andrews, A. E.: Evaluation of MOPITT Retrievals of Lowertropospheric Carbon Monoxide over the United States, J. Geophys. Res., 117, D13306, doi:10.1029/2012JD017553, 2012.

Deeter, M. N., Martínez-Alonso, S., Edwards, D. P., Emmons, L. K., Gille, J. C., Worden, H. M., Pittman, J. V., Daube, B. C., and Wofsy, S. C.: Validation of MOPITT Version 5 thermal-infrared, near-infrared, and multispectral carbon monoxide profile retrievals for 2000–2011, J. Geophys. Res., 118, 1–16, doi:10.1002/jgrd.50272, 2013.

de Laat, A. T. J., Gloudemans, A. M. S., Aben, I., Krol, M., Meirink, J. F., van der Werf, G. R., and Schrijver, H.: Scanning Imaging Absorption Spectrometer for Atmospheric Chartography carbon monoxide total columns: Statistical evaluation and comparison with chemistry transport model results, J. Geophys. Res., 112, D12310, doi:10.1029/2006JD008256, 2007.

de Meij, A., Pozzer, A., and Lelieveld, J.: Trend analysis in aerosol optical depths and pollutant emission estimates between 2000 and 2009, Atmos. Environ., 51, 75–85, doi:10.1016/j.atmosenv.2012.01.059, 2012.

Dlugokencky, E. J., Dutton, E. G., Novelli, P. C., Tans, P. P., Masarie, K. A., Lantz, K. O., and Madronich, S.: Changes in methane and CO growth rates after the eruption of Mt. Pinatubo and their link with changes in tropical tropospheric UV flux, Geophys. Res. Lett., 23, 2761–2764, doi:10.1029/96GL02638, 1996.

Drummond, J. R. and Mand, G. S.: The measurements of pollution in the troposphere (MOPITT) instrument: Overall performance and calibration requirements, J. Atmos. Ocean Tech., 13, 314–320, 1996.

Duncan, B. N. and Logan, J. A.: Model analysis of the factors regulating the trends and variability of carbon monoxide between 1988 and 1997, Atmos. Chem. Phys., 8, 7389–7403, doi:10.5194/acp-8-7389-2008, 2008.

Duncan, B. N., Logan, J. A., Megretskaia, I. A., Yantosca, R. M., Novelli, P. C., Jones, N. B., and Rinsland, C. P.: The global budget of CO, 1988–1997: source estimates and validation with a global model, J. Geophys. Res.-Atmos., 112, D22301, doi:10.1029/2007JD008459, 2007.

Ehhalt, D., Prather, M., Dentener, F., Derwent, R., Dlugokencky, E., Holland, E., Isaksen, I., Katima, J., Kirchhoff, V., Matson, P., Midgley, P., and Wang, M.: Atmospheric chemistry and greenhouse gases, in: Climate Change 2001: The Scientific Basis, Contribution of Working Group I to the Third Assessment Report of the Intergovernmental Panel on Climate Change, edited by: Houghton, J. T., Ding, Y., Griggs, D. J., Noguer, M., van der Linden, P. J., Dai, X., Maskell, K., and Johnson, C. A., Cambridge University Press, Cambridge, UK, 257–259, 2001.

Emmons, L. K., Deeter, M. N., Gille, J. C., Edwards, D. P., Attié, J.-L., Warner, J., Ziskin, D., Francis, G. , Khattatov, B., Yudin, V., Lamarque, J.-F., Ho, S.-P., Mao, D., Chen, J. S., Drummond, J., Novelli, P., Sachse, G., Coffey, M. T., Hannigan, J. W., Gerbig, C. , Kawakami, S., Kondo, Y., Takegawa, N., Schlager, H., Baehr, J., and Ziereis, H.: Validation of Measurements of Pollution in the Troposphere (MOPITT) CO retrievals with aircraft in situ profiles, J. Geophys. Res., 109, D03309, doi:10.1029/2003JD004101, 2004.

Eskes, H. J. and Boersma, K. F.: Averaging kernels for DOAS total-column satellite retrievals, Atmos. Chem. Phys., 3, 1285–1291, doi:10.5194/acp-3-1285-2003, 2003.

Facchini, M. C., Decesari, S., Mircea, M., Fuzzi, S., and Loglio, G.: Surface tension of atmospheric wet aerosol and cloud/fog droplets in relation to their organic carbon econtent and chemical composition, Atmos. Environ., 33, 4853–4857, 2000.

Fishman, J. and Crutzen, P. J.: the origin of ozone in the troposphere, Nature, 274, 855–858, 1978.

Forster, P., Ramaswamy, V., Artaxo, P., Berntsen, T., Betts, R., Fahey, D. W., Haywood, J., Lean, J., Lowe, D. C., Myhre, G., Nganga, J., Prinn, R., Raga, G., Schulz, M., and Van Dorland, R.: Changes in Atmospheric Constituents and in Radiative Forcing. In: Climate Change 2007: The Physical Science Basis. Contribution of Working Group I to the Fourth Assessment Report of the Intergovernmental Panel on Climate Change, edited by: Solomon, S., Qin, D., Manning, M., Chen, Z., Marquis, M., Averyt, K. B., Tignor, M., and Miller, H. L., Cambridge University Press, Cambridge, United Kingdom and New York, NY, USA, 129–234, 2007.

George, M., Clerbaux, C., Hurtmans, D., Turquety, S., Coheur, P.-F., Pommier, M., Hadji-Lazaro, J., Edwards, D. P., Worden, H., Luo, M., Rinsland, C., and McMillan, W.: Carbon monoxide distributions from the IASI/METOP mission: evaluation with other space-borne remote sensors, Atmos. Chem. Phys., 9, 8317–8330, doi:10.5194/acp-9-8317-2009, 2009.

Giglio, L., Randerson, J. T., van der Werf, G. R., Kasibhatla, P. S., Collatz, G. J., Morton, D. C., and DeFries, R. S.: Assessing variability and long-term trends in burned area by merging

multiple satellite fire products, Biogeosciences, 7, 1171–1186, doi:10.5194/bg-7-1171-2010, 2010.

Gomez-Pelaez, A. J., Ramos, R., Gomez-Trueba, V., Novelli, P. C., and Campo-Hernandez, R.: A statistical approach to quantify uncertainty in carbon monoxide measurements at the Izaña global GAW station: 2008–2011, Atmos. Meas. Tech., 6, 787–799, doi:10.5194/amt-6-787-2013, 2013.

Graniera, C., Müller, J. F., Pétron, G., and Brasseur, G.: A three-dimensional study of the global CO budget, Chemosphere, 1, 255–261, doi:10.1016/S1465-9972(99)00007-0, 1999.

Granier, C., Bessagnet, B., Bond, T., D'Angiola, A., van der Gon, H. D., Frost, G. J., Heil, A., Kaiser, J. W., Kinne, S., Klimont, Z., Kloster, S., Lamarque, J.-F., Liousse, C., Masui, T., Meleux, F., Mieville, A., Ohara, T., Raut, J.-C., Riahi, K., Schultz, M. G., Smith, S. J., Thompson, A., van Aardenne, J., van der Werf, G. R., and van Vuuren, D. P.: Evolution of anthropogenic and biomass burning emissions of air pollutants at global and regional scales during the 1980-2010 period, Clim. Change, 109, 163–190, doi:10.1007/s10584-011-0154-1, 2011.

Haas-Laursea, D. and Hartley, D.: Consistent sampling methods for comparing models to CO_2 flask data, J. Geophys. Res., 102, 19059–19071, doi:10.1029/97JD00795, 1997.

Hauglustaine, D. A., Brasseur, G. P., Walters, S., Rasch, P. J., Müller, J.-F., Emmons, L. K., and Carroll, M. A.: MOZART, a global chemical transport model for ozone and related chemical tracers: 2. Model results and evaluation, J. Geophys. Res., 103, 28291–28335, doi:10.1029/98JD02398, 1998.

Held, I. M., Delworth, T. L., Lu, J., Findell, K. L., and Knutson, T. R.: Simulation of Sahel drought in the 20th and 21st centuries, P. Natl. Acad. Sci. USA, 102, 17891–17896, doi:10.1073/pnas.0509057102, 2005.

Hilboll, A., Richter, A., and Burrows, J. P.: Long-term changes of tropospheric NO_2 over megacities derived from multiple satellite instruments, Atmos. Chem. Phys., 13, 4145–4169, doi:10.5194/acp-13-4145-2013, 2013.

Ho, S.-P., Edwards, D. P., Gille, J. C., Luo, M., Osterman, G. B., Kulawik, S. S., and Worden, H.: A global comparison of carbon monoxide profiles and column amounts from Tropospheric Emission Spectrometer (TES) and Measurements of Pollution in the Troposphere (MOPITT), J. Geophys. Res., 114, D21307, doi:10.1029/2009JD012242, 2009.

Hogrefe, C., Lynn, B., Civerolo, K., Ku, J., Rosenthal, J., Rosenzweig, C., Goldberg, R., Gaffin, S., Knowlton, K., and Kinney, P.: Simulating changes in regional air pollution over the eastern United States due to changes in global and regional climate and emissions, J. Geophys. Res, 109, D22301, doi:10.1029/2004JD004690, 2004.

Holloway, T., Levy II, H., and Kasibhatla, P.: Global distribution of carbon monoxide, J. Geophys. Res., 105, 12123–12147, doi:10.1029/1999JD901173, 2000.

Hooghiemstra, P. B., Krol, M. C., Meirink, J. F., Bergamaschi, P., van der Werf, G. R., Novelli, P. C., Aben, I., and Röckmann, T.: Optimizing global CO emission estimates using a four-dimensional variational data assimilation system and surface network observations, Atmos. Chem. Phys., 11, 4705–4723, doi:10.5194/acp-11-4705-2011, 2011.

Hsu, N. C., Gautam, R., Sayer, A. M., Bettenhausen, C., Li, C., Jeong, M. J., Tsay, S.-C., and Holben, B. N.: Global and regional trends of aerosol optical depth over land and ocean using SeaWiFS measurements from 1997 to 2010, Atmos. Chem. Phys., 12, 8037–8053, doi:10.5194/acp-12-8037-2012, 2012.

Intergovernmental Panel on Climate Change (IPCC): Climate Change 1995, University Press, Cambridge, UK, 1996.

Jacobson, M. and Streets, D.: Influence of future anthropogenic emissions on climate, natural emissions, and air quality, J. Geophys. Res., 114, D08118, doi:10.1029/2008JD011476, 2009.

Jeuken, A. B. M., Siegmund, P. C., Heijboer, L. C., Feichter, J., and Bengtsson, L.: On the potential of assimilating meteorological analyses in a global climate model for the purpose of model validation, J. Geophys. Res., 101, 16939–16950, doi:10.1029/96JD01218, 1996.

Jöckel, P., Tost, H., Pozzer, A., Brühl, C., Buchholz, J., Ganzeveld, L., Hoor, P., Kerkweg, A., Lawrence, M. G., Sander, R., Steil, B., Stiller, G., Tanarhte, M., Taraborrelli, D., van Aardenne, J., and Lelieveld, J.: The atmospheric chemistry general circulation model ECHAM5/MESSy1: consistent simulation of ozone from the surface to the mesosphere, Atmos. Chem. Phys., 6, 5067–5104, doi:10.5194/acp-6-5067-2006, 2006.

Jöckel, P., Kerkweg, A., Pozzer, A., Sander, R., Tost, H., Riede, H., Baumgaertner, A., Gromov, S., and Kern, B.: Development cycle 2 of the Modular Earth Submodel System (MESSy2), Geosci. Model Dev., 3, 717–752, doi:10.5194/gmd-3-717-2010, 2010.

Johnson, B. T., Osborne, S. R., Haywood, J. M., and Harrison, M. A. J.: Aircraft measurements of biomass burning aerosol over West Africa during DABEX, J. Geophys. Res., 113, D00C06, doi:10.1029/2007JD009451, 2008.

Khalil, M. A. K. and Rasmussen, R. A.: Carbon monoxide in the Earth's atmosphere: indications of a global increase, Nature, 332, 242–245, doi:10.1038/332242a0, 1988.

Khalil, M. A. K. and Rasmussen, R. A.: The global cycle of carbon monoxide: trends and mass balance, Chemosphere, 20, 227–242, 1990.

Kirby, K. R., Laurance, W. F., Albernaz, A. K., Schroth, G., Fearnside, P. M., Bergen, S., Venticinque, E. M., and da Costa, C.: The future of deforestation in the Brazilian Amazon, Futures, 38, 432–453, doi:10.1016/j.futures.2005.07.011, 2006.

Klonecki, A., Pommier, M., Clerbaux, C., Ancellet, G., Cammas, J.-P., Coheur, P.-F., Cozic, A., Diskin, G. S., Hadji-Lazaro, J., Hauglustaine, D. A., Hurtmans, D., Khattatov, B., Lamarque, J.-F., Law, K. S., Nedelec, P., Paris, J.-D., Podolske, J. R., Prunet, P., Schlager, H., Szopa, S., and Turquety, S.: Assimilation of IASI satellite CO fields into a global chemistry transport model for validation against aircraft measurements, Atmos. Chem. Phys., 12, 4493–4512, doi:10.5194/acp-12-4493-2012, 2012.

Kopacz, M., Jacob, D. J., Fisher, J. A., Logan, J. A., Zhang, L., Megretskaia, I. A., Yantosca, R. M., Singh, K., Henze, D. K., Burrows, J. P., Buchwitz, M., Khlystova, I., McMillan, W. W., Gille, J. C., Edwards, D. P., Eldering, A., Thouret, V., and Nedelec, P.: Global estimates of CO sources with high resolution by adjoint inversion of multiple satellite datasets (MOPITT, AIRS, SCIAMACHY, TES), Atmos. Chem. Phys., 10, 855–876, doi:10.5194/acp-10-855-2010, 2010.

Latif, M. and Keenlyside, N. S.: El Niño/Southern Oscillation response to global warming, P. Natl. Acad. Sci. USA, 106, 20578–20583, doi:10.1073/pnas.0710860105, 2009.

Law, K. S.: Theoretical studies of carbon monoxide distributions, budgets and trends, Chemosphere – Global Change Science, 1, 19–31, doi:10.1016/S1465-9972(99)00020-3, 1999.

Lawrence, M. G., Jöckel, P., and von Kuhlmann, R.: What does the global mean OH concentration tell us?, Atmos. Chem. Phys., 1, 37–49, doi:10.5194/acp-1-37-2001, 2001.

Leggett, J., Pepper, W. J., and Swart, R. J.: Emissions scenarios for the IPCC: an update, in: Climate Change 1992: The Supplementary Report to the IPCC Scientific Assessment, prepared by: IPCC Working Group I, edited by: Houghton, J. T., Callander, B. A., and Varney, S. K. and WMO/UNEP, Cambridge University Press, Cambridge, UK, and New York, NY, USA, 1992.

Lelieveld, J., Peters, W., Dentener, F. J., and Krol, M. C.: Stability of tropospheric hydroxyl chemistry, J. Geophys. Res., 107, ACH 17-1–ACH 17-11, doi:10.1029/2002JD002272, 2002.

Lelieveld, J., Dentener, F. J., Peters, W., and Krol, M. C.: On the role of hydroxyl radicals in the self-cleansing capacity of the troposphere, Atmos. Chem. Phys., 4, 2337–2344, doi:10.5194/acp-4-2337-2004, 2004.

Lelieveld, J., Barlas, C., Giannadaki, D., and Pozzer, A.: Model calculated global, regional and megacity premature mortality due to air pollution, Atmos. Chem. Phys., 13, 7023–7037, doi:10.5194/acp-13-7023-2013, 2013.

Levy, H.: Normal atmosphere: large radical and formaldehyde concentrations predicted, Science, 173, 141–143, doi:10.1126/science.173.3992.141, 1971.

Junhua Liu, Logan, J. A., Jones, D. B. A., Livesey, N. J., Megretskaia, I., Carouge, C., and Nedelec, P.: Analysis of CO in the tropical troposphere using Aura satellite data and the GEOS-Chem model: insights into transport characteristics of the GEOS meteorological products, Atmos. Chem. Phys., 10, 12207–12232, doi:10.5194/acp-10-12207-2010, 2010.

Logan, J. A., Prather, M. J., Wofsy, S. C., and McElroy, M. B.: Tropospheric chemistry: A global perspective, J. Geophys. Res., 86, 7210–7254, doi:10.1029/JC086iC08p07210, 1981.

Lu, Z., Streets, D. G., Zhang, Q., Wang, S., Carmichael, G. R., Cheng, Y. F., Wei, C., Chin, M., Diehl, T., and Tan, Q.: Sulfur dioxide emissions in China and sulfur trends in East Asia since 2000, Atmos. Chem. Phys., 10, 6311–6331, doi:10.5194/acp-10-6311-2010, 2010.

Luo, M., Rinsland, C. P., Rodgers, C. D., Logan, J. A., Worden, H., Kulawik, S., Eldering, A., Goldman, A., Shephard, M. W., Gunson, M., and Lampel, M.: TES carbon monoxide validation with DACOM aircraft measurements during INTEX-B 2006, J. Geophys. Res., 112, D24S48, doi:10.1029/2007JD008803, 2007a.

Luo, M., Rinsland, C. P., Rodgers, C. D., Logan, J. A., Worden, H., Kulawik, S., Eldering, A., Goldman, A., Shephard, M. W., Gunson, M., and Lampel, M.: Comparison of carbon monoxide measurements by TES and MOPITT: Influence of a priori data and instrument characteristics on nadir atmospheric species retrievals, J. Geophys. Res., 112, D09303, doi:10.1029/2006JD007663, 2007b.

McFiggans, G., Alfarra, M., Allan, J., Bower, K., and Coe, H.: Simplification of the representation of the organic component of atmospheric particulates, Faraday Discuss., 130, 341–362, doi:10.1039/b419435g, 2005.

Meehl, G. A., Covey, C., Delworth, T., Latif, M., McAvaney, B., Mitchell, J. F. B., Stouffer, R. J., and Taylor, K. E.: The WCRP CMIP3 multimodel dataset: A new era in climate change research, B. Am. Meteorol. Soc., 88, 1383–1394, doi:10.1175/BAMS-88-9-1383, 2007.

Meinshausen, M., Smith, S. J., Calvin, K., Daniel, J. S., Kainuma, M. L. T., Lamarque, J.-F., Matsumoto, K., Montzka, S. A., Raper, S. C. B., Riahi, K., Thomson, A., Velders, G. J. M., and van Vuuren, D. P. P.: The RCP greenhouse gas concentrations and their extensions from 1765 to 2300, Clim. Change, 109, 213–241, doi:10.1007/s10584-011-0156-z, 2011.

Nakicenovic, N., Alcamo, J., Davis, G., De Vries, B., Fenhann, J., Gaffin, S., Gregory, K., Grübler, A., Jung, T. Y., Kram, T., Lebre La Rovere, E., Michaelis, L., Mori, S., Morita, T., Pepper, W., Pitcher, H., Price, L., Riahi, K., Roehrl, A., Rogner, H. H., Sankovski, A., Schlesinger, M., Priyadarshi Shukla, P., Smith, S., Swart, R., Van Rooijen, S., Victor, N., and Dadi, Z.: Special Report on Emissions Scenarios, Intergovernmental Panel on Climate Change, 599 pp., Cambridge University press, Cambridge, United Kingdom and New York, USA, 2000.

Novelli, P. C., Steele, L. P., and Tans, P. P.: Mixing ratios of carbon monoxide in the troposphere, J. Geophys. Res., 97, 20731–20750, doi:10.1029/92JD02010, 1992.

Novelli, P. C., Masarie, K. A., Tans, P. P., and Lang, P. M.: Recent Changes in Atmospheric Carbon Monoxide, Science, 263, 1587–1590, doi:10.1126/science.263.5153.1587, 1994.

Novelli, P. C., Masarie, K. A., Lang, P. M., Hall, B. D., Myers, R. C., and Elkins, J. W.: Reanalysis of tropospheric CO trends: Effects of the 1997–1998 wildfires, J. Geophys. Res., 108, 4464, doi:10.1029/2002JD003031, 2003.

Ohara, T., Akimoto, H., Kurokawa, J., Horii, N., Yamaji, K., Yan, X., and Hayasaka, T.: An Asian emission inventory of anthropogenic emission sources for the period 1980–2020, Atmos. Chem. Phys., 7, 4419–4444, doi:10.5194/acp-7-4419-2007, 2007.

Pan, L., Edwards, D. P., Gille, J. C., Smith, M. W., and Drummond, J. R.: Satellite remote sensing of tropospheric CO and CH_4: forward model studies of the MOPITT instrument, Appl. Optics, 34, 6976–6988, doi:10.1364/AO.34.006976, 1995.

Pan, L., Gille, J. C., Edwards, D. P., Bailey, P. L., and Rodgers, C. D.: Retrieval of tropospheric carbon monoxide for the MOPITT experiment, J. Geophys. Res., 103, 32277–32290, doi:10.1029/98JD01828, 1998.

Pozzer, A., Jöckel, P., Tost, H., Sander, R., Ganzeveld, L., Kerkweg, A., and Lelieveld, J.: Simulating organic species with the global atmospheric chemistry general circulation model ECHAM5/MESSy1: a comparison of model results with observations, Atmos. Chem. Phys., 7, 2527–2550, doi:10.5194/acp-7-2527-2007, 2007.

Pozzer, A., Jöckel, P., and Van Aardenne, J.: The influence of the vertical distribution of emissions on tropospheric chemistry, Atmos. Chem. Phys., 9, 9417–9432, doi:10.5194/acp-9-9417-2009, 2009.

Pozzer, A., de Meij, A., Pringle, K. J., Tost, H., Doering, U. M., van Aardenne, J., and Lelieveld, J.: Distributions and regional budgets of aerosols and their precursors simulated with the EMAC chemistry-climate model, Atmos. Chem. Phys., 12, 961–987, doi:10.5194/acp-12-961-2012, 2012a.

Pozzer, A., Zimmermann, P., Doering, U. M., van Aardenne, J., Tost, H., Dentener, F., Janssens-Maenhout, G., and Lelieveld, J.: Effects of business-as-usual anthropogenic emissions on air quality, Atmos. Chem. Phys., 12, 6915–6937, doi:10.5194/acp-12-6915-2012, 2012b.

Rasmusson, E. M. and Carpenter, T. H.: Variations in Tropical Sea Surface Temperature and Surface Wind Fields Associated with the Southern Oscillation/El Niño, Mon. Weather Rev., 110, 354–384, doi:10.1175/1520-0493(1982)110<0354:VITSST>2.0.CO;2, 1982.

Reeves, C. E., Formenti, P., Afif, C., Ancellet, G., Attié, J.-L., Bechara, J., Borbon, A., Cairo, F., Coe, H., Crumeyrolle, S., Fierli, F., Flamant, C., Gomes, L., Hamburger, T., Jambert, C., Law, K. S., Mari, C., Jones, R. L., Matsuki, A., Mead, M. I., Methven, J., Mills, G. P., Minikin, A., Murphy, J. G., Nielsen, J. K., Oram, D. E., Parker, D. J., Richter, A., Schlager, H., Schwarzenboeck, A., and Thouret, V.: Chemical and aerosol characterisation of the troposphere over West Africa during the monsoon period as part of AMMA, Atmos. Chem. Phys., 10, 7575–7601, doi:10.5194/acp-10-7575-2010, 2010.

Riahi, K., Gruebler, A., and Nakicenovic, N.: Scenarios of long-term socio-economic and environmental development under climate stabilization, Technol. Forecast. Soc., 74, 887–935, doi:10.1016/j.techfore.2006.05.026, 2007.

Richter, A., Burrows, J. P., Nüß, H., Granier, C., and Niemeier, U.: Increase in tropospheric nitrogen dioxide over China observed from space, Nature Letters, 437, 129–132, doi:10.1038/nature04092, 2005.

Rieder, H. E., Frossard, L., Ribatet, M., Staehelin, J., Maeder, J. A., Di Rocco, S., Davison, A. C., Peter, T., Weihs, P., and Holawe, F.: On the relationship between total ozone and atmospheric dynamics and chemistry at mid-latitudes – Part 2: The effects of the El Niño/Southern Oscillation, volcanic eruptions and contributions of atmospheric dynamics and chemistry to long-term total ozone changes, Atmos. Chem. Phys., 13, 165–179, doi:10.5194/acp-13-165-2013, 2013.

Rodgers, C. D.: Inverse methods for atmospheric sounding – theory and practice, Series on Atmospheric, Oceanic and Planetary Physics, World Scientific Publishing, Singapore, 2000.

Rodgers, C. D. and Connor, B. J.: Intercomparison of Remote Sounding Instruments, J. Geophys. Res., 108, 4116, doi:10.1029/2002JD002299, 2003.

Roeckner, E., Brokopf, R., Esch, M., Giorgetta, M., Hagemann, S., Kornblueh, L., Manzini, E., Schlese, U., and Schulzweida, U.: Sensitivity of simulated climate to horizontal and vertical resolution in the ECHAM5 atmosphere model, J. Climate, 19, 3771–3791, doi:10.1175/JCLI3824.1, 2006.

Smith, S. J., Pitcher, H., and Wigley, T. M. L.: Global and regional anthropogenic sulfur dioxide emissions, Global Planet. Change, 29, 99–119, doi:10.1016/S0921-8181(00)00057-6, 2001.

Streets, D. G., Bond, T. C., Carmichael, G. R., Fernandes, S. D., Fu, Q., He, D., Klimont, Z., Nelson, S. M., Tsai, N. Y., Wang, M. Q., Woo, J. -H., and Yarber, K. F.: An inventory of gaseous and primary aerosol emissions in Asia in the year 2000, J. Geophys. Res., 108, 8809, doi:10.1029/2002JD003093, 2003.

Streets, D. G., Wu, Y., and Chin, M.: Two-decadal aerosol trends as a likely explanation of the global dimming/brightening transition, Geophys. Res. Lett., 33, L15806, doi:10.1029/2006GL026471, 2006.

Taylor, K. E.: Summarizing multiple aspects of model performance in a single diagram, J. Geophys. Res., 106, 7183–7192, doi:10.1029/2000JD900719, 2001.

Thompson, A. M.: The oxidizing capacity of the Earth's atmosphere-Probable past and future changes, Science, 256, 1157–1165, doi:10.1126/science.256.5060.1157, 1992.

Thompson, A. M. and Cicerone, R. J.: Possible perturbations to atmospheric CO, CH_4, and OH, J. Geophys. Res., 91, 10853–10864, doi:10.1029/JD091iD10p10853, 1986.

Tiao, G. C., Reinsel, G. C., Xu, D., Pedrick, J. H., Zhu, X., Miller, A. J., DeLuisi, J. J., Mateer, C. L., and Wuebbles, D. J.: Effects of autocorrelation and temporal sampling schemes on estimates of trend and spatial correlation, J. Geophys. Res., 95, 20507–20517, doi:10.1029/JD095iD12p20507, 1990.

Tohjima, Y., Kubo, M., Minejima, C., Mukai, H., Tanimoto, H., Ganshin, A., Maksyutov, S., Katsumata, K., Machida, T., and Kita, K.: Temporal changes in the emissions of CH4 and CO from China estimated from CH_4/CO_2 and CO/CO_2 correlations observed at Hateruma Island, Atmos. Chem. Phys., 14, 1663–1677, doi:10.5194/acp-14-1663-2014, 2014.

Trenberth, K. E., Caron, J. M., Stepaniak, D. P., and Worley, S.: Evolution of El Niño-Southern Oscillation and global atmospheric surface temperatures, J. Geophys. Res., 107, 4065, doi:10.1029/2000JD000298, 2002.

University of Toronto and NCAR MOPITT Team: MOPITT (Measurement of Pollution in the Troposphere) Level 1 Algorithm Theoretical Basis Documents, ATBD-MOP-01, University of Toronto and NCAR MOPITT Team, http://eospso.gsfc.nasa.gov/sites/default/files/atbd/atbd-mop-01.pdf (last access: 19 September 2014), 1–45, August, 1996.

van der Werf, G. R., Randerson, J. T., Giglio, L., Collatz, G. J., Mu, M., Kasibhatla, P. S., Morton, D. C., DeFries, R. S., Jin, Y., and van Leeuwen, T. T.: Global fire emissions and the contribution of deforestation, savanna, forest, agricultural, and peat fires (1997–2009), Atmos. Chem. Phys., 10, 11707–11735, doi:10.5194/acp-10-11707-2010, 2010.

van Vuuren, D. P., Eickhout, B., Lucas, P. L., and den Elzen M. G. J.: Long-Term Multi-Gas Scenarios to Stabilise Radiative Forcing – Exploring Costs and Benefits Within an Integrated Assessment Framework, The Energy Journal, Special issue #3, 201–234, doi:10.5547/ISSN0195-6574-EJ-VolSI2006-NoSI3-10, 2006.

van Vuuren, D. P., den Elzen, M. G. J., Lucas, P. L., Eickhout, B., Strengers, B. J., van Ruijven, B., Wonink, S., and van Houdt, R.: Stabilizing greenhouse gas concentrations at low levels: an assessment of reduction strategies and costs, Clim. Change, 81, 119–159, doi:10.1007/s10584-006-9172-9, 2007.

van Vuuren, D. P., Edmonds, J. A., Kainuma, M., Riahi, K., Thomson, A. M., Hibbard, K., Hurtt, G. C., Kram, T., Krey, V., Lamarque, J.-F., Masui, T., Nakicenovic, M. M. N., Smith, S. J., and Rose, S.: The representative concentration pathways: an overview, Clim. Change, 109, 5–31, doi:10.1007/s10584-011-0148-z, 2011.

Wallace, J. M., and Hobbs, P. V.: Atmospheric Chemistry, in: Atmospheric Science, Second Edition: An Introductory Survey, edited by: Dmowska, R., Hartmann, D., and Rossby, H. T., Elsevier, MA, USA, California, USA, and London, UK, 153–207, 2006.

Weatherhead, E. C., Reinsel, G. C., Tiao, G. C., Meng, X.-L., Choi, D., Cheang, W.-K., Keller, T., DeLuisi, J., Wuebbles, D. J., Kerr, J. B., Miller, A. J., Oltmans, S. J., and Frederick, J. E.: Factors affecting the detection of trends: Statistical considerations and applications to environmental data, J. Geophys. Res., 103, 17149–17161, doi:10.1029/98JD00995, 1998.

Weatherhead, E. C., Stevermer, A. J., and Schwartz, B. E.: Detecting environmental changes and trends, Physics and Chemistry of the Earth, 27, 399–403, doi:10.1016/S1474-7065(02)00019-0, 2002.

WMO: Scientific Assessment of Ozone Depletion: 1998. Global Ozone Research and Monitoring Project – Report No. 44, World Meteorological Organization, Geneva, Switzerland, 732 pp., 1999.

WMO: Revision of the World Data Centre for Greenhouse Gases Data Submission and Dissemination Guide, GAW Report No. 188, WMO TD No.1507, World Meteorological Organization, Geneva, Switzerland, 49 pp., 2009.

Worden, H. M., Deeter, M. N., Edwards, D. P., Gille, J. C., Drummond, J. R., and Nédélec, P. P.: Observations of near-surface carbon monoxide from space using MOPITT multispectral retrievals, J. Geophys. Res., 115, D18314, doi:10.1029/2010JD014242, 2010.

Worden, H. M., Deeter, M. N., Frankenberg, C., George, M., Nichitiu, F., Worden, J., Aben, I., Bowman, K. W., Clerbaux, C., Coheur, P. F., de Laat, A. T. J., Detweiler, R., Drummond, J. R., Edwards, D. P., Gille, J. C., Hurtmans, D., Luo, M., Martínez-Alonso, S., Massie, S., Pfister, G., and Warner, J. X.: Decadal record of satellite carbon monoxide observations, Atmos. Chem. Phys., 13, 837–850, doi:10.5194/acp-13-837-2013, 2013.

Xu, X., Lin, W., Wang, T., Yan, P., Tang, J., Meng, Z., and Wang, Y.: Long-term trend of surface ozone at a regional background station in eastern China 1991–2006: enhanced variability, Atmos. Chem. Phys., 8, 2595–2607, doi:10.5194/acp-8-2595-2008, 2008.

Yoon, J., von Hoyningen-Huene, W., Vountas, M., and Burrows, J. P.: Analysis of linear long-term trend of aerosol optical thickness derived from SeaWiFS using BAER over Europe and South China, Atmos. Chem. Phys., 11, 12149–12167, doi:10.5194/acp-11-12149-2011, 2011.

Yoon, J., von Hoyningen-Huene, W., Kokhanovsky, A. A., Vountas, M., and Burrows, J. P.: Trend analysis of aerosol optical thickness and Ångström exponent derived from the global AERONET spectral observations, Atmos. Meas. Tech., 5, 1271–1299, doi:10.5194/amt-5-1271-2012, 2012.

Yoon, J., Pozzer, A., Hoor, P., Chang, D. Y., Beirle, S., Wagner, T., Schloegl, S., Lelieveld, J., and Worden, H. M.: Technical Note: Temporal change in averaging kernels as a source of uncertainty in trend estimates of carbon monoxide retrieved from MOPITT, Atmos. Chem. Phys., 13, 11307–11316, doi:10.5194/acp-13-11307-2013, 2013.

Yoon, J., Burrows, J. P., Vountas, M., von Hoyningen-Huene, W., Chang, D. Y., Richter, A., and Hilboll, A.: Changes in atmospheric aerosol loading retrieved from space-based measurements during the past decade, Atmos. Chem. Phys., 14, 6881–6902, doi:10.5194/acp-14-6881-2014, 2014.

Zhang, Y., Yu, H., Eck, T. F., Smirnov, A., Chin, M., Remer, L. A., Bian, H., Tan, Q., Levy, R., Holben, B. N., and Piazzolla, S.: Aerosol Daytime Variations over North and South America Derived from Multiyear AERONET Measurements, J. Geophys. Res., 117, D05211, doi:10.1029/2011JD017242, 2012.

Zhao, T. X.-P., Laszlo, I., Guo, W., Heidinger, A., Cao, C., Jelenak, A., Tarpley, D., and Sullivan, J.: Study of long-term trend in aerosol optical thickness observed from operational AVHRR satellite instrument, J. Geophys. Res., 113, D07201, doi:10.1029/2007JD009061, 2008.